

N 70 27 140
NASA CR 109853

NATIONAL AERONAUTICS AND SPACE ADMINISTRATION

Technical Report 32-1427

*Compatibility and Shielding Analysis of Science
Instruments in Spacecraft Containing a
Radioisotope Thermoelectric
Generator*

C. G. Miller

V. C. Truscello

CASE FILE
COPY

JET PROPULSION LABORATORY
CALIFORNIA INSTITUTE OF TECHNOLOGY
PASADENA, CALIFORNIA

May 1, 1970

NATIONAL AERONAUTICS AND SPACE ADMINISTRATION

Technical Report 32-1427

*Compatibility and Shielding Analysis of Science
Instruments in Spacecraft Containing a
Radioisotope Thermoelectric
Generator*

C. G. Miller

V. C. Truscello

JET PROPULSION LABORATORY
CALIFORNIA INSTITUTE OF TECHNOLOGY
PASADENA, CALIFORNIA

May 1, 1970

Preface

The work described in this report was performed by the Guidance and Control Division of the Jet Propulsion Laboratory.

Contents

I. Introduction	1
II. Relevant Characteristics of RTG, Spacecraft, and Experiment Components	2
A. Radiation Spectra of the RTG	2
1. Neutron radiation	3
2. Gamma radiation	4
B. Modes of Action of Science Instrument Components	5
1. Charged particle detectors	5
2. Neutral particle detectors	5
3. Photon detectors	5
4. Magnetic field detectors	5
5. Photomultiplier tubes	5
III. Description of the Science Experiments	5
IV. Approach	8
V. Analytic Model of Sensitive Components	9
A. Solid-State Detectors	9
B. Geiger-Mueller Tubes	10
C. Photomultiplier Tubes and Channeltrons	12
VI. Neutron and Gamma-Photon Spectra of the RTG	12
A. Change of Spectrum as a Function of Time	12
B. Modification of Spectrum by Shielding	14
VII. Shielding Requirements and Effectiveness	16
A. Optimization of Shielding Weight	16
B. Shielding Requirements	16
1. Channeltrons and Geiger counters	18
2. Solid-state detectors	21
C. Summary	23
VIII. Current Programs	23
References	25

Contents (contd)

Tables

1. Expected neutron yield of RTG fuel based on available Pu ²³⁸	2
2. Radiation levels at various distances from the surface of the Cronus RTG operating at 4100 W (thermal) or 300 W (electrical)	3
3. Damage threshold for representative electronic components	3
4. Injection transistor gain degradation from neutrons	4
5. Susceptibility of science instruments to RTG radiation	6
6. Investigators for the <i>Mariner Mars</i> 1964 science experiments	8
7. Number of photons/cm ² required to deposit 1 R	9
8. Absorption probabilities for gamma photons encountering silicon and germanium	11
9. Surface gamma-photon flux of Cronus RTG	13
10. Surface neutron flux of Cronus RTG	13
11. Characteristics of RTG-grade Pu ²³⁸	13
12. Gamma-photon spectra for RTG at various times after plutonium separation (normalized to 1.0 for the 0.5- to 1.0-MeV energy interval at 18 yr)	14
13. Mass-absorption coefficients for uranium μ'_{U} and tungsten μ'_{W} for the 0.2- to 8-MeV energy interval	15
14. Contribution of capture gammas produced in tungsten shielding to total emerging gamma photons	15
15. Ratio of emerging to incident gamma-photon flux	19
16. Effect of tungsten shielding on spurious counting rate for Channeltrons and Geiger counters	20
17. Effect of tungsten shielding on spurious counting rate for silicon solid-state detectors	22
18. Effect of tungsten shielding on the number of gamma photons absorbed from incident beam by a germanium slab	22
19. Weight of shielding required for science experiments in the vicinity of the Cronus RTG	23

Contents (contd)

Figures

1. Comparison of spectra of neutrons arising from spontaneous fission and from (α,n) reactions	2
2. Representative group of science instruments (carried on <i>Mariner Mars 1964</i> mission)	7
3. Probability of absorption of gamma photons in 0.3-cm-thick silicon and germanium detectors	10
4. Number of secondary electrons traversing Geiger counter as a result of impinging photons	10
5. Experimental curves for the counting efficiency of Geiger-Mueller tubes with brass walls	11
6. Conceptual design of an RTG (<i>Martin-Marietta Cronus</i> model)	12
7. Gamma and neutron field intensity at various distances from the RTG	14
8. Gamma-photon spectrum at various times after separation of the Pu^{238} fuel	14
9. Mass absorption coefficients between 0.5 and 6 MeV as a function of atomic number	15
10. Intensity distribution of gamma photons produced by neutron-flux interaction with various thicknesses of tungsten	16
11. Total gamma-photon field of RTG for various thicknesses of tungsten (sum of total emerging and capture gammas)	16
12. Relative response vs gamma-photon energy for Geiger counters and Channeltrons with various thicknesses of tungsten	17
13. Relative response vs gamma-photon energy for silicon solid-state detectors with various thicknesses of tungsten	17
14. Relative response vs gamma-photon energy for germanium solid-state detectors with various thicknesses of tungsten	17
15. Dose rate vs photon energy (0.01–10 MeV)	18
16. Photon flux vs energy (0.01–10 MeV)	18
17. Secondary electron emission coefficient (extrapolated from Fig. 5 data)	19
18. Effect of ¼-in. increments of tungsten shielding on the ratio of spurious counts in Geiger counters and Channeltrons	20
19. Background counting rate for Channeltrons (CEM-401, CEM-4010) caused by the Cronus RTG with various thicknesses of tungsten shielding	20

Contents (contd)

Figures (contd)

20. Background counting rate for Geiger–Mueller tube (EON-6213) caused by the Cronus RTG with various thicknesses of tungsten shielding 21
21. Effect of ¼-in. increments of tungsten shielding on the ratio of spurious counts in silicon and germanium solid-state detectors 22
22. Background counting rate for 12-mm² × 31.7-μm silicon cell caused by the Cronus RTG 24
23. Background counting rate for 5.7-cm² × 200-μm silicon cell caused by the Cronus RTG 24

Abstract

The use of radioisotope thermoelectric generators as a solar-independent power source in spacecraft is considered. The probability of misinterpretation of generator-produced neutron and gamma fields for naturally occurring phenomena by onboard science instruments is investigated (it was recognized that gamma-photon radiation is the main source of interference). Spatial deployment and shielding requirements are discussed.

Geiger-Mueller tubes, electron multipliers, and silicon surface-barrier detectors are evaluated in detail. Because the sensitivity of the science instruments varies with the energy of the radiation, a 20-group structure in the 0.04- to 10-MeV range was developed to determine the spectral distribution of the radiation energy. Analytic models are developed to predict the effect of these spectra on the instruments selected. The possible degradation of spacecraft electronics is also investigated.

The principal findings were that the gamma-photon field does affect the operation of the instruments (which would require shielding), while the neutron field does not—either directly or indirectly through capture-gamma production. The age of the fuel is a factor in determining the amount of background interference. The degradation threshold for most electrical components is above the level produced by the fuel. A marginal case exists for injection transistors; methods are proposed for alleviating this condition. The analysis and conclusions presented here are being refined by further analytical studies and an experimental program currently underway at JPL.

Compatibility and Shielding Analysis of Science Instruments in Spacecraft Containing a Radioisotope Thermoelectric Generator

I. Introduction

Space missions to date have depended on solar panels for electrical power. The current state-of-the-art capability of solar panels is an output of 10 W/lb at a distance of 1 AU from the sun. At Jupiter (5.2 AU) and Saturn (9.5 AU), the output of solar panels drops to 0.5 and 0.1 W/lb, respectively. Foreseeable developments are not expected to increase this rating by more than a factor of three.

Among the solar-independent power sources that have been considered are the radioisotope thermoelectric generator (RTG) and the radioisotope thermionic generator (RTIG). For missions longer than a month in duration, the most promising system (on the basis of energy and power available per unit mass) is the RTG. At present, the RTG can produce approximately 1 W/lb. This rating matches present solar-panel capability at a distance of 3 AU from the sun.

The distinctive characteristics of an RTG in spacecraft applications that are considered herein are the result of the incidental but ever-present neutron and gamma radi-

ation fields that accompany the RTG. In fact, the major objection to the use of an RTG is the potential interference with the scientific equipment in the spacecraft. This is because the radiation from the RTG may affect an experiment in a manner that cannot easily be distinguished from the desired signal. Several experiments are examined in this report to determine which are sensitive to RTG radiation and, of those that are, what corrective measures can be taken to avoid spurious interactions with the generator. Possible corrective measures are the use of coincidence techniques, correction for background values, and additional shielding. However, any measure will exact a penalty in weight, complexity, or reliability. The emphasis of this report is on instrument sensitivity, shielding requirements, and spatial deployment.

Additionally, it is well known that neutron and gamma fields can cause specific materials to degrade. However (despite the complicating factors of gradually decreasing power output, changing radiation spectra, and decay-product buildup), much is known about this type of degradation and the engineering techniques required to overcome it are available.

II. Relevant Characteristics of RTG, Spacecraft, and Experiment Components

The instrument selected to measure a particular phenomenon may be adversely affected by RTG-generated radiation. For example, certain elements of an optical instrument may darken upon exposure to gamma radiation, and pulses caused by gamma or neutron radiation from the RTG may be difficult for a particle detector to distinguish from those pulses caused by external particle flux. Examples of detectors susceptible to gamma and neutron radiation are: (1) scintillation devices, (2) surface-barrier, solid-state devices, and (3) ionization chambers.

In practice, most of the instruments for the science experiments do not depend on particle ionization or emission to function. Equally important is the fact that many of the experiments measure electromagnetic radiation at wavelengths different from those caused by an RTG, or phenomena completely unrelated to the type of field produced by an RTG. Examples of experiments that measure different wavelengths include: (1) microwave, (2) visual and ultraviolet radiometers and spectrometers, (3) radio propagation and occultation experiments, and (4) television experiments. Examples of experiments that measure phenomena unrelated to an RTG are: (1) micrometeoroid detectors and (2) cosmic dust collectors.

A. Radiation Spectra of the RTG

The gamma and the neutron fields in the vicinity of an RTG originate primarily from the radioactivity of the Pu^{238} and associated radioactive nuclides in the heat source. The gamma field is caused mainly by the plutonium isotopes and their daughter products in the heat source. A small additional contribution to the gamma field is caused by the interaction of emitted neutrons and any construction or shielding material encountered. The neutron field is primarily caused by (α, n) reactions with impurities associated with the PuO_2 in the heat source. A smaller contribution to the neutron flux is caused by the (α, n) reaction with the O^{18} in the PuO_2 , and the smallest neutron contribution is made by the spontaneous fission of the plutonium content. Table 1 shows the approximate contribution of the three sources of neutron flux. Figure 1 compares the spectrum of neutrons arising from spontaneous fission with the spectrum of neutrons from the (α, n) reactions. The differences are not significant in connection with potential interference from the RTG. The neutron flux level from an RTG could be decreased by reducing the level of impurities or by replacing the O^{18} with O^{16} , or both. In practice, the neutron flux levels from present fuels, as shown in Table 1, contribute only a small portion

Table 1. Expected neutron yield of RTG fuel based on available Pu^{238}

Origin of neutrons	Practical expected yield, n/g-s	
	Minimum	Maximum
Spontaneous fission	2,100	2,100
Reaction (α, n) from O^{18} in PuO_2	11,300	11,300
Reaction (α, n) from impurities in Pu^{238}		
Lower range of impurities, parts/ 10^6		
B-100	4,100	
Na-600	1,300	
Mg-100	200	
Al-100	100	
Upper range of impurities, parts/ 10^6		
B-6400		262,000
Na-7600		16,700
Mg-9000		18,900
Al-3500		3,500
Total (per gram of contained plutonium)	19,100	314,500

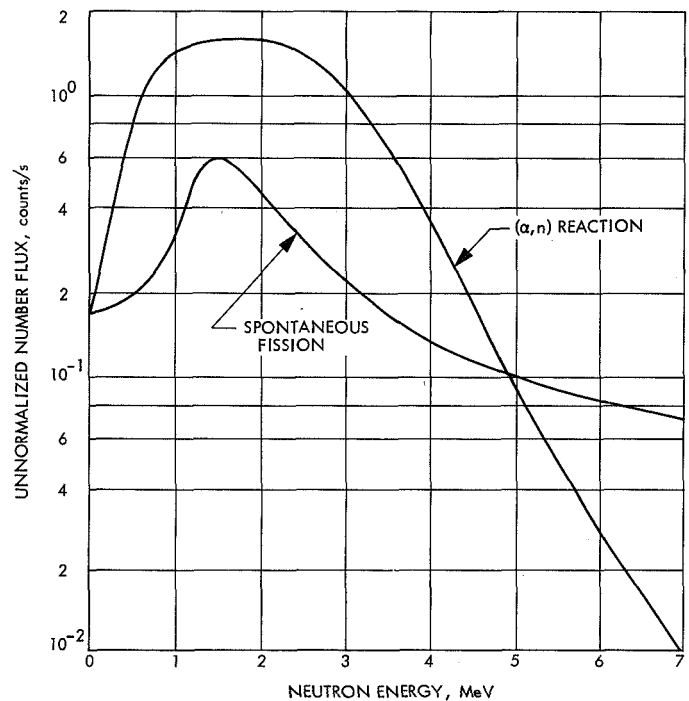


Fig. 1. Comparison of spectra of neutrons arising from spontaneous fission and from (α, n) reactions

of the interference with the science experiments. An effort to reduce the gamma field levels would be more profitable.

1. Neutron radiation. The long-term radiation degradation effects of the neutron cumulative dose is a more serious influence than the cumulative gamma dose. The level of radiation at various distances from the RTG is shown in Table 2. Gamma radiation is expressed in terms of millirads per hour, whereas the neutron component of the radiation is given in terms of neutrons per square centimeter per second.

At 3 ft from the surface of the RTG, the neutron level is 1600 n/cm^2 -s, and the gamma level is 63 mrad/h. For a 10-yr mission, the total integrated neutron flux will be $5.1 \times 10^{11} n/cm^2$ and the total integrated gamma flux will be 5.5×10^8 rad at a distance of 3 ft. Correspondingly larger or smaller doses will occur for lesser and greater separations (see Table 2).

Table 2. Radiation levels at various distances from the surface of the Cronus RTG operating at 4100 W (thermal) or 300 W (electrical)

Distance from surface		mrad/h	n/cm^2 -s
cm	ft		
0	0	903	53,700
12.5	0.41	634	22,500
22.5	0.74	421	13,200
32.5	1.07	288	8,490
42.5	1.4	206	5,900
82.5	2.7	76	2,100
91.4	3	63	1,600
122.5	4.01	38.5	1,020
152.4	5	26.3	860
202.5	6.64	15.4	430
213.4	7	14.0	380
242.5	7.95	10.9	320
274.3	9	8.5	230
335.3	11	5.7	160
396.2	13	4.1	110
457.2	15	3.05	90

Table 3 gives the threshold of damage, representing the point at which one can expect a measurable decrease in component performance; however, a 50% performance degradation would probably not occur until the dose is a factor of 100 higher than the threshold value. In all cases, the gamma-radiation component is below the threshold value.

Table 3. Damage threshold for representative electronic components

Component	Rad	n/cm^2
<i>Injection transistors</i>	10^5	
min		3×10^{10}
max		2×10^{12}
<i>Diodes</i>	10^6	5×10^{12}
<i>Field-effect transistors</i>	10^5	2×10^{13}
<i>Microcircuits</i>	10^7	10^{14}
<i>Silicon-controlled rectifiers</i>	10^7	10^{12}
<i>Capacitors</i>		
min	10^4	3×10^{12}
max	10^7	10^{15}
<i>Resistors</i>	10^7	10^{15}
<i>Transformers and inductors</i>	10^7	10^{16}

The neutron component of radiation is also below the threshold value of most electronic components. The one notable exception is the injection transistor. In general, these transistors have threshold values above $3 \times 10^{11} n/cm^2$ (Table 4); however, two (2N930 and 2N1724) have values as low as $3 \times 10^{10} n/cm^2$. This marginal condition can be alleviated in a number of ways:

- (1) Select transistors with a high damage threshold.
- (2) Design the circuit to allow for operation with a 70% degradation in transistor gain (applicable for switching transistors) so that radiation will not affect normal operation. All of the transistors will show much less than a 50% degradation in gain (Table 4) at the expected neutron flux levels.
- (3) Increase the distance between sensitive components and the RTG whenever possible.
- (4) Remove some of the impurities in the plutonium heat source. In principle, shielding can be used to reduce neutron levels, but it is difficult to shield broad-spectrum neutrons. Shielding to reduce neutron levels generally carries a larger weight penalty than is justified by the decrease in neutron dose.

The present report and analysis is based on the Cronus RTG, which is a plutonium-fueled generator. Because the power density of plutonium is 0.4 W/g, and the radioactive content of a Cronus RTG is 10,250 g of plutonium, the generator is rated at 4100 W (thermal) or 300 W (electrical). The fuel for the Cronus RTG is specified to have a neutron output of $4.1 \times 10^4 n/g$ -s or a total output of $(4.1 \times 10^4)(1.025 \times 10^4) = 4.2 \times 10^8 n/s$.

From Table 1 it is seen that present chemical capability exists to produce fuel sources that are lower by a factor of two in specific neutron output than the Cronus RTG. One improvement that is considered feasible but has not yet been carried to the production stage consists of reducing the O¹⁸ content of the PuO₂ by O¹⁶ exchange. Current estimates are that the O¹⁸ content can be reduced to 20% of the present level, thus reducing the 11,300-n/g-s contribution (indicated in Table 1) to 2260 n/g-s, making a total of 10,060 n/g-s for minimum impurity fuel using O¹⁸-depleted PuO₂. Possible improvements beyond this point are based on experiments with "high-purity plutonium." This purification scheme (used to produce ultra-high purity Pu²³⁹), is known as the Lamex process (Ref. 1). If applied successfully to Pu²³⁸, it would permit production of fuel with an "impurity element" (α, n) contribution (other than the residual O¹⁸ contribution) of 500 n/g-s, for a total output of about 5000 n/g-s. The sequence of improved specific neutron outputs may be tabulated as follows:

Method	Output, n/g-s
Present Cronus RTG	4×10^4
Best present chemical practice	2×10^4
Reduction of O ¹⁸ content to 20% of present level (developmental process)	1×10^4
Purification by Lamex process (developmental)	0.5×10^4

The impact of these decreased neutron fluxes will be apparent only in terms of an improvement in long-term radiation degradation effects. For the present, it can be stated that permanently damaging effects to electronic components and spacecraft subsystems are, at worst, marginal for certain sensitive components and negligible for the majority of the components.

2. Gamma radiation. Of greater concern is the problem of operating the science instruments in an RTG environment. Interference with science experiments in the spacecraft is due almost entirely to the gamma-photon flux. The gamma-photon flux is changed only slightly by the rigorous purification processes outlined in Subsection A-1.

The sensors that may respond to RTG radiation and show a background reading even in the absence of any

Table 4. Injection transistor gain degradation from neutrons

Transistor	Threshold of degradation, n/cm ²	50% degradation, n/cm ²
2N930	3×10^{10}	2×10^{12}
2N2412	8×10^{11}	4×10^{13}
2N2369	10^{12}	3×10^{13}
2N708	2×10^{12}	7×10^{13}
2N910	3×10^{11}	10^{13}
2N915	10^{12}	4×10^{13}
2N956	4×10^{11}	10^{13}
2N1893	4×10^{11}	2×10^{13}
2N1613	6×10^{11}	2×10^{13}
2N3251	3×10^{11}	10^{13}
2N2060	10^{12}	4×10^{12}
2N2604	7×10^{11}	3×10^{13}
2N2907A	4×10^{11}	2×10^{13}
2N914	2×10^{12}	5×10^{13}
2N1973	3×10^{11}	10^{13}
2N2297	10^{12}	4×10^{13}
2N2222	4×10^{11}	10^{13}
2N2034	7×10^{10}	3×10^{12}
2N2150	7×10^{10}	3×10^{12}
2N1724	3×10^{10}	2×10^{12}
2N2331	10^{12}	4×10^{13}
2N2432	10^{11}	7×10^{12}
MM/2N491/ B(UJT)	2×10^{11}	10^{12}
2N2642	10^{12}	4×10^{12}
2N2807	10^{12}	4×10^{12}

real signal will, in practice, be placed at a distance from the RTG. In addition, local heavy-metal shielding will be used at each sensor so that the effects of the RTG radiation will be kept at an acceptably low level. The use of heavy-metal shielding modifies the gamma spectrum because the low-energy photons are preferentially removed from the spectrum. To a much smaller degree, the energies of some photons that are not captured in the shielding are modified and decreased in energy. Thus, the net removal of low-energy photons is not as efficient as would be indicated by the simple application of an absorption coefficient.

An additional source of change in the gamma-photon spectrum is aging. Freshly separated plutonium fuel has a spectrum that has a predominance of low-energy photons. As the plutonium fuel continues to generate heat, the decay products of the small Pu²³⁶ impurity increases the number of photons in the 2- to 3-MeV group, relative to the more easily shielded peak output of "young" Pu²³⁸, which produces photons in the 0.7- to 0.8-MeV range.

B. Modes of Action of Science Instrument Components*

The spacecraft science instrumentation may be broadly classified according to the type of phenomenon it is designed to detect or measure:

- (1) Positive particle detectors.
- (2) Negative particle detectors.
- (3) Neutron detectors.
- (4) Radio-frequency measurements.
- (5) Optical and near-optical frequency measurements.
- (6) X- and gamma-ray measurements.
- (7) Magnetic-field measurements.

The seven general types of instruments listed above will be briefly discussed in terms of their radiation susceptibility, but first some general observations are in order. Any instrument that depends upon particle ionization for its operation is particularly susceptible to RTG radiation. This includes scintillation devices; surface-barrier, solid-state detectors; and ionization chambers. Although gamma photons generally produce more spurious counts than neutrons in the unshielded case, the difficulty in shielding against neutrons makes them a more serious problem in the long run. The primary neutron-induced problems arise from: (1) the production of secondary gamma photons in materials close to the detecting device because of inelastic neutron scattering and (n,γ) reactions, and (2) the direct interaction of neutrons with the detecting material, producing high-energy displacements as well as subatomic particles.

1. Charged particle detectors. These detectors include electrostatic, electromagnetic, and ionization devices. The first two types (Langmuir-type probes, RF impedance probes, Faraday cups, and electromagnetic analyzers) are inherently "hard" to RTG radiation provided that they are properly oriented with respect to the RTG. They are, however, susceptible to spacecraft charge effects. They are not suitable for many applications, and for these, ionization-type detectors must be used.

The surface-barrier, gold-silicon detectors are superior to the large-volume scintillation detectors because of the reduced probability of a neutron or gamma photon interaction with the smaller detector volume. In general, instruments specifically designed to detect electrons employ

*The material in this subsection was abstracted from an unpublished report prepared by the Martin Marietta Corp.

smaller detector volumes; therefore, they are less susceptible to RTG effects.

2. Neutral particle detectors. These devices include mass spectrometers and hot- or cold-cathode ionization gages. This type of instrument is not appreciably affected by spurious RTG radiation because the number of electrons necessarily generated by the instrument to induce ionization is far in excess of the number that would be generated by the secondary processes associated with the absorption of RTG radiations.

3. Photon detectors. No RTG-caused interference is expected with devices measuring electromagnetic radiation at optical or greater wavelengths. These instruments include radiometers and such optical devices as telescopes and television cameras. At shorter wavelengths, RTG interference can be expected, however, especially with instruments designed to detect X- and gamma rays.

4. Magnetic field detectors. These devices include both flux-gate magnetometers and the helium-plasma magnetometer. Neither type of magnetometer is susceptible to RTG radiation, although allowance must be made for the stray magnetic fields that might emanate from the RTG if definitive magnetic-field measurements are to be performed.

5. Photomultiplier tubes. Although not generally used as radiation detectors directly, photomultiplier tubes are an inherent part of scintillation counters and other devices that must respond to photon pulses in the optical region.

Thresholds have been established for gamma-photon-induced conductivity in some types of photomultiplier tubes. This induced conductivity is from two major sources: (1) luminescence induced in the glass envelope and (2) increased electron density in the vicinity of the first few dynodes due to Compton scattering of the gamma photons. Testing has indicated that at least 5×10^6 gammas/cm²-s at 1 MeV are required to produce measurable conductivity. This gamma-photon flux is in excess of the number expected from an RTG at distances greater than $3\frac{1}{4}$ ft (1 m).

III. Description of the Science Experiments

The experiments that may compose a science package for a multiplanet mission are listed in Table 5. The table indicates whether a particular experiment will be affected by RTG radiation. Six of the experiments are insensitive

Table 5. Susceptibility of science instruments to RTG radiation

Experiment	Effect	Sensitive element	Remarks
Micrometeoroid detector	None		
Television	None		
Infrared radiometer	None		Requires simple radiant shielding
Infrared interferometer	None		Requires simple radiant shielding
Solar plasma probe	None		
Magnetometer	None		
LEPEDEA ^a	Possible	Channeltron photomultiplier and Geiger-Mueller tube	Acceptable for particle flux measurement in the vicinity of planets. Interference possible if used to measure smaller fluxes in interplanetary environments
UV photometer	Possible	Channeltron photomultiplier and Geiger-Mueller tube	Possible interference from secondary emission if entrance area is unshielded
Trapped radiation detector	Yes	Solid-state and Geiger-Mueller tube	
Cosmic ray and energetic solar charged particle experiment	Yes	Solid-state (Li-drift Si)	RTG causes 500x space rate for low energy (single channel)
		Plastic scintillation counter	Small loss using coincidence
		Photomultiplier to read plastic scintillation counter	Sensitive photomultiplier tubes may give false responses due to gamma-induced luminescence in glass envelope or false count from Compton-scattered electrons in vicinity of initial dynode

^aLEPEDEA = low-energy proton and electron differential energy analyzer.

to RTG radiation, and two others are affected only under certain conditions. Among the latter two, the low-energy proton and electron differential energy analyzer (LEPEDEA) experiment will suffer interference only if this device is used to measure the small flux of electrons and protons that exists within the interplanetary environment. Generally, this instrument would be used to measure the charged-particle environment surrounding the target planets. Under these conditions, the particle fluxes are several orders of magnitude above the RTG radiation levels. A representative group of instruments is shown in Fig. 2, that consists of those instruments carried on the *Mariner Mars 1964* mission (Ref. 2). The investigators involved in this flight and their affiliations are given in Table 6.

The first six experiments listed in Table 5 (the micrometeoroid detector, the television system, the infrared radiometer, the infrared interferometer, the solar plasma probe, and the helium magnetometer) are not expected to have any interference from RTG radiation, and are suitable for use without shielding or special consideration.

The seventh experiment, the LEPEDEA, is described in detail in Ref. 3. This instrument utilizes cylindrical, curved-plate electrostatic analyzers to provide measurements of the differential energy spectra of protons and electrons within, and in the vicinity of, the magnetosphere of the earth. Continuous-channel multipliers (Channeltrons), which are used to count individual charged particles accepted by the analyzers, provide the instrument with a dynamic range in proton and electron intensities extending from 10^4 to 10^{10} particles/cm²-s-sr in a given energy bandpass of the electrostatic analyzer. The widths of the energy bandpasses of the electrostatic analyzers are sufficient to cover the entire energy range from 90 to 70,000 eV (protons and electrons separately) in 14 voltage steps on the curved plates. The four electrostatic analyzers (two analyzers each for protons and electrons to cover the above energy range)—complete with signal conditioner, high-voltage power supplies, and thermal shell—have an average power requirement of 2 W and weigh 6.3 lb.

The eighth experiment is the ultraviolet photometer. The wavelength regions of interest are the He I line at

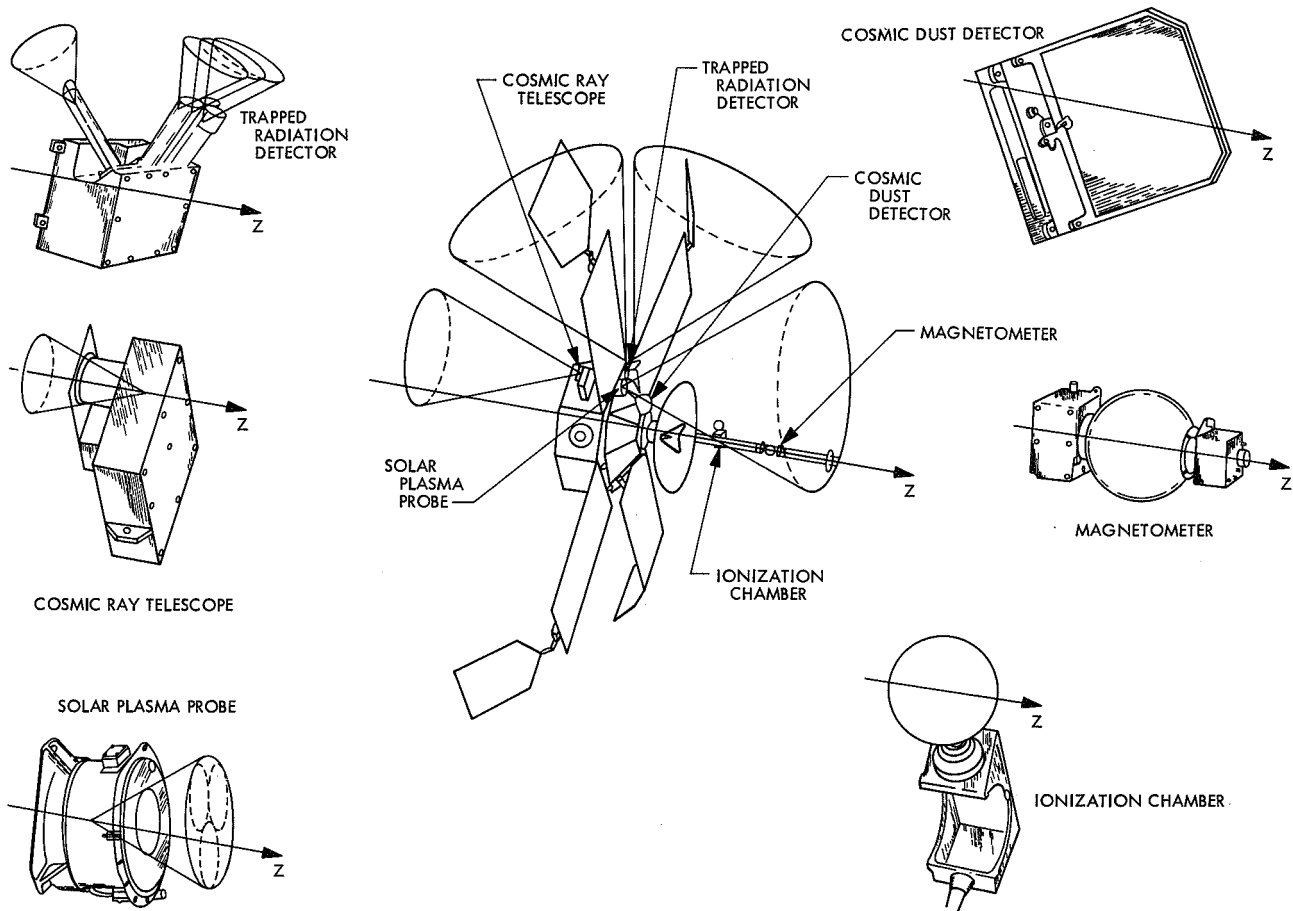


Fig. 2. Representative group of science instruments (carried on *Mariner Mars 1964* mission)

Table 6. Investigators for the Mariner Mars 1964 science experiments

Experiment	Investigators	Affiliation
Television	Leighton, R. B. ^a	CIT
	Murray, B. C.	CIT
	Sharp, R. P.	CIT
	Sloan, R. K.	JPL
	Allen, J. D.	JPL
Helium magnetometer	Smith, E. J. ^a	JPL
	Coleman, P. J., Jr.	UCLA
	Davis, L., Jr.	CIT
	Jones, D. E.	Brigham Young University and JPL
Cosmic dust detector	Alexander, W. M. ^a	Goddard Space Flight Center
	Berg, O. E.	Goddard Space Flight Center
	McCracken, C. W.	Goddard Space Flight Center
	Secretan, L.	Goddard Space Flight Center
	Bohn, J. L. Fuchs, O. P.	Temple University Temple University
Ionization chamber	Neher, H. V. ^a	CIT
	Anderson, H. R.	JPL
Cosmic ray telescope	Simpson, J. A. ^a	University of Chicago
	O'Gallagher, J.	University of Chicago
Trapped radiation detector	Van Allen, J. A. ^a	State University of Iowa
	Frank, L. A.	State University of Iowa
	Krimijis, S. M.	State University of Iowa
Solar plasma probe	Bridge, H. L. ^a	MIT
	Lazarus, A.	MIT
	Snyder, C. W.	JPL
Occultation	Kliore, A. J. ^a	JPL
	Cain, D. L.	JPL
	Levy, G. S.	JPL
	Fableman, V. R.	Stanford University
	Fjeldbo, G. Drake, F.	Stanford University Cornell University

^aPrincipal investigator.

584 Å, the He II line at 304 Å, the H α line at 1215 Å, and the O I line at 1305 Å. The secondary electrons ejected from a photocathode are amplified by passage through a channel multiplier. A combination of appropriate optical filters and surface preparation of the photocathodes will make each channel responsive only to the intended radiation, holding the dark current to under 1 count/s.

The ninth experiment is the trapped radiation detector. The radiation to be detected consists of the charged particles (protons and electrons) that are trapped near a planet by the magnetic field of that planet. If the sensors are sensitive enough and the RTG interference level is low enough, the detector can also measure the nontrapped, free flux of charged particles in interplanetary space. The detecting elements consist of the thin-window Geiger-Mueller tubes to detect electrons with energies of 40 KeV and a solid-state, surface-barrier detector. The surface-barrier detector measures proton flux in the energy range of 0.5 to 10 MeV.

The tenth experiment is the cosmic ray and energetic solar charged particle experiment, which is designed to measure the flux and determine an energy spectrum for protons and alpha particles in the interplanetary environment. Protons are detected and recorded in the energy spectrum from 1 to 180 MeV. Correspondingly, alpha particles from 2 to 360 MeV are recorded. The experiment has directional discrimination; therefore, it can measure the flux magnitude, the energy distribution, and the direction of the proton and alpha particle constituents of primary cosmic rays.

IV. Approach

The approach that was used to evaluate instrument sensitivity and develop the shielding requirements is outlined as follows:

- (1) Instruments that were suspected of being affected by the RTG radiation were selected for evaluation.
- (2) A thorough study of the operation and description of these instruments was made to determine the sensitive components and the dimensions of the sensitive volumes. The minimum charged-particle counting rate of each detector was also established.
- (3) Because the sensitivity of the detector to RTG radiation (gamma and neutron) varies with the energy of the radiation, an accurate spectral description of the emitted radiation is necessary. The following spectral information was determined in the form of a 20-group structure:
 - (a) Magnitude and description of both the neutrons and gamma photons emitted by the radiation source at various points outside the RTG envelope.
 - (b) Reduction in magnitude and change in spectral distribution of the gamma-photon radiation as

a result of placing various thicknesses of tungsten shielding between the RTG and detector.

- (c) Magnitude and spectrum of the gamma-photon radiation produced by the interaction of the neutrons with the shielding material.
- (4) A suitable analytical model was developed to predict the effects of the radiation spectra of item (3) on the following sensitive components:
 - (a) Solid-state detectors.
 - (b) Geiger-Mueller tubes.
 - (c) Continuous-channel multipliers.
- (5) An acceptable value of spurious counting was established.
- (6) The data from the analytical model and the established values of allowable interference were used to determine the amount of shielding required for each of the experiments consisting of one or more of the above (item 4) radiation-sensitive components.

V. Analytic Model of Sensitive Components

A. Solid-State Detectors

The trapped radiation detector and the cosmic ray and energetic solar charged particle experiment (experiments 9 and 10) use the effect of charged-particle interaction in the depleted zone of a solid-state detector. Gamma photons traversing the depletion zone do not register directly; however, they are registered indirectly and in an energy-dependent fashion because photoelectrons, Compton-scattered electrons, or pair-produced electrons or positrons are liberated when a gamma photon interacts with the silicon or germanium material in the detector. These liberated electrons may then register a count in the same manner that a desired event would otherwise do in such a system.

A study made by Jones (Ref. 4) gives experimental information on the counting rates of silicon junctions for gamma photons of 0.1- and 0.4-MeV energies. These data enable normalization of the calculated relative response of silicon and germanium detectors; they also enable determination of the contribution of the different energy portions of the RTG gamma-photon fields to the backgrounds of the solid-state detectors when used in experiments 9 and 10.

The data points given in Ref. 4 were based on the use of a silicon *p-i-n* junction 100-mm² × 500-μm deep. Jones

observed 10⁸ counts/R at 0.1 MeV and 10⁷ counts/R at 0.4 MeV. One roentgen corresponds to the production of 2.08 × 10⁹ ion pairs in 1 cm³ of air. If the energy to produce one ion pair is 33.5 eV, then 6.97 × 10⁴ MeV/cm³ is the energy absorbed per roentgen dose in that cubic centimeter.

To determine the number of gamma photons needed to deliver 6.97 × 10⁴ MeV/cm³, use is made of the absorption coefficient μ_{α} (in cm⁻¹) because $\mu_{\alpha}E_{\gamma}$ is the energy in millions of electron volts absorbed per gamma photon per centimeter of path length. This absorption coefficient gives the fractional part of the photon energy loss per centimeter. The total absorption coefficient is equal to the sum of the absorption coefficients for: (1) the photoelectric effect, (2) incoherent Compton scattering, and (3) pair production—multiplied, in each case, by the fraction of the energy given to an electron in the process. Using the absorption coefficients given by White (Ref. 5), the number of photons/cm² equal to 1 R is given in Table 7.

The work done in Ref. 4 showed that, with a particular silicon *p-i-n* junction, 10⁸ counts/R were given at 0.1 MeV and 10⁷ counts/R at 0.4 MeV. Using the values in Table 7, 10⁸ counts/R at 0.1 MeV is 10⁸ counts/2.36 × 10¹⁰ gamma photons, or 0.0042 count/gamma photon. Similarly, 10⁷ counts/R at 0.4 MeV is 10⁷ counts/4.60 × 10⁹ gamma photons, or 0.0022 count/gamma photon at this energy.

Table 7. Number of photons/cm² required to deposit 1 R

Photon energy E_{γ} , MeV	γ/cm^2
5	5.88 × 10 ⁸
4	7.06 × 10 ⁸
3	8.47 × 10 ⁸
2	1.15 × 10 ⁹
1	1.93 × 10 ⁹
0.9	2.12 × 10 ⁹
0.8	2.30 × 10 ⁹
0.7	2.65 × 10 ⁹
0.6	3.03 × 10 ⁹
0.5	3.65 × 10 ⁹
0.4	4.60 × 10 ⁹
0.3	6.23 × 10 ⁹
0.2	1.01 × 10 ¹⁰
0.1	2.36 × 10 ¹⁰
0.09	2.65 × 10 ¹⁰
0.08	2.86 × 10 ¹⁰
0.07	3.11 × 10 ¹⁰
0.06	3.11 × 10 ¹⁰

The absorption probabilities for germanium and silicon resulting from photoelectric, Compton-scattering, and pair-production contributions are shown in Fig. 3; these data were adapted from Goulding (Ref. 6). Based on the data shown in Fig. 3, the total probability of absorption of a photon for each of 20 selected energies is given in Table 8 for silicon and germanium. Not every absorption event leads to a count because the depth of the depletion region and the threshold voltage in the detector electronics affect the counting efficiency. In the measurement at 0.1 MeV (see Ref. 4), there was 0.0042 count/gamma photon, although the absorption probability from Table 8 is 0.125. Thus, the possibility of recording a liberated electron is $0.0042/0.125 = 3.4\%$ at 0.1 MeV. Similarly, at 0.4 MeV, there was 0.0022 count/gamma photon, and the absorption probability from Table 8 is 0.064. The probability of recording a liberated electron is $0.0022/0.064 = 3.4\%$ at 0.4 MeV, which is the same as the probability at 0.1 MeV. The 3.4% probability, which can be expected to be constant for the complete gamma spectrum of interest, relates only to the measurement (see Ref. 4) on a 500- μm -thick depletion zone. For other thicknesses, the response will be proportional to the thickness of the depleted zone. In practice, an experimental, one-point determination is most desirable for determining the background to be expected from a given gamma-photon flux intensity of known spectral distribution. In this manner, it is possible to calculate

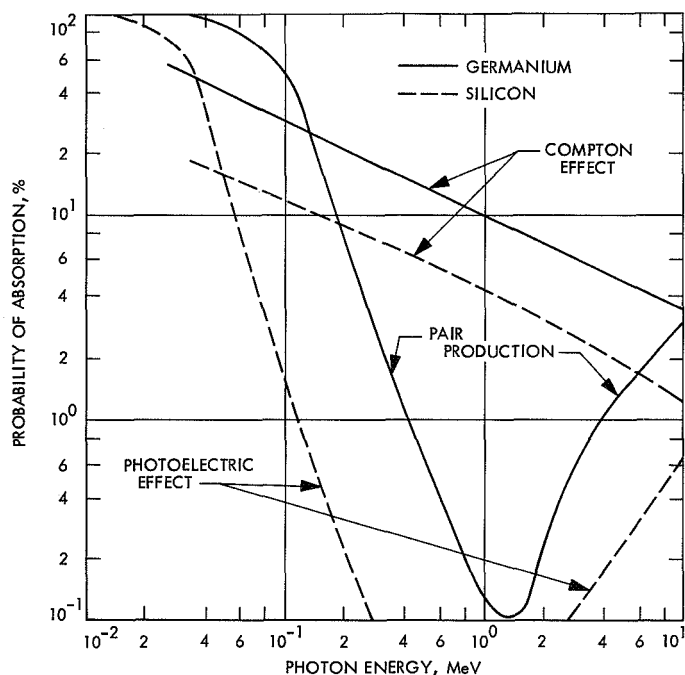


Fig. 3. Probability of absorption of gamma photons in 0.3-cm-thick silicon and germanium detectors

the interference in a solid-state detector caused by a gamma-photon flux of known energy spectrum. This is done by multiplying the flux at each energy by the corresponding probability of interaction (taken from Table 8), taking into account the thickness of the depleted zone, its area, and the number of counts expected per gamma photon.

It should be noted that the probability of interaction falls rapidly with increasing gamma-photon energy. The interactions of the lowest energy gamma photons, which potentially give the greatest interference, are those of the gamma-photon radiations that are most easily shielded by heavy-metal shielding.

B. Geiger-Mueller Tubes

The LEPEDEA, the UV photometer, and the trapped radiation detector (experiments 7-9) use Geiger-Mueller tubes in conjunction with Channeltrons or solid-state detectors. The response of the Geiger-Mueller tube to gamma photons impinging on it is due almost entirely to those secondary electrons produced in the tube wall that penetrate into the sensitive volume of the tube. Much information is available concerning the response of Geiger-Mueller tubes to gamma photons of various energies, as a function of cathode wall material (Refs. 7 and 8).

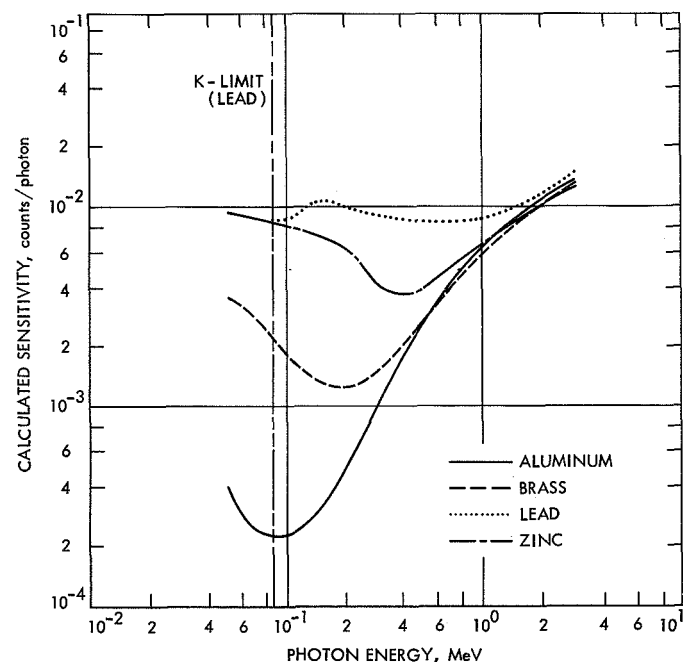


Fig. 4. Number of secondary electrons traversing Geiger counter as a result of impinging photons

Table 8. Absorption probabilities for gamma photons encountering silicon and germanium

Photon energy E_γ , MeV	Silicon				Germanium			
	Photo-electric effect	Compton scattering	Pair production	Total probability	Photo-electric effect	Compton scattering	Pair production	Total probability
0.04	0.30	0.17	—	0.47	0.90	0.42	—	(1.320)
0.1	0.015	0.11	—	0.125	0.42	0.28	—	0.700
0.25	0.001	0.075	—	0.076	0.032	0.16	—	0.192
0.35	—	0.068	—	0.068	0.013	0.15	—	0.163
0.45	—	0.060	—	0.060	0.008	0.13	—	0.138
0.55	—	0.053	—	0.053	0.045	0.12	—	0.124
0.65	—	0.05	—	0.050	0.003	0.11	—	0.113
0.75	—	0.048	—	0.048	0.0022	0.105	—	0.107
0.85	—	0.046	—	0.046	0.0018	0.10	—	0.102
0.95	—	0.042	—	0.042	0.0014	0.098	—	0.099
1.1	—	0.040	—	0.040	0.001	0.09	—	0.091
1.3	—	0.036	—	0.036	—	0.082	0.001	0.083
1.5	—	0.033	—	0.033	—	0.080	0.0012	0.081
1.7	—	0.031	—	0.031	—	0.075	0.0017	0.077
1.9	—	0.030	—	0.030	—	0.070	0.0021	0.072
2.5	—	0.026	0.001	0.027	—	0.06	0.004	0.064
3.5	—	0.021	0.0014	0.022	—	0.052	0.0085	0.060
4.5	—	0.020	0.002	0.022	—	0.047	0.012	0.059
5.5	—	0.015	0.003	0.018	—	0.042	0.015	0.057
6.5	—	0.014	0.004	0.018	—	0.040	0.02	0.060

The Geiger-Mueller tube that will be used in the science experiments has a stainless-steel wall, and the potential interference with the science experiments will be from secondary electrons produced in this wall by gamma photons from the RTG. A theory developed by von Droste (Ref. 9) gives the number of secondary electrons traversing the Geiger counter, as a result of impinging photons, for aluminum ($Z = 13$), brass ($Z = 29$), zinc ($Z = 30$), or lead ($Z = 82$) cathodes (Fig. 4). For gamma photons more energetic than 0.3 MeV, the curves relating to brass ($Z = 29$) may be used for calculations of stainless-steel cathodes ($Z = 26$). Experimental curves for the number of secondary electrons produced by photon interaction with the walls of a Geiger counter (Ref. 7), for brass cathodes, are shown in Fig. 5. These curves are in reasonable agreement with the theory of von Droste (see Ref. 9).

The contribution of gamma photons less energetic than 0.3 MeV is not appreciable because any shielding used

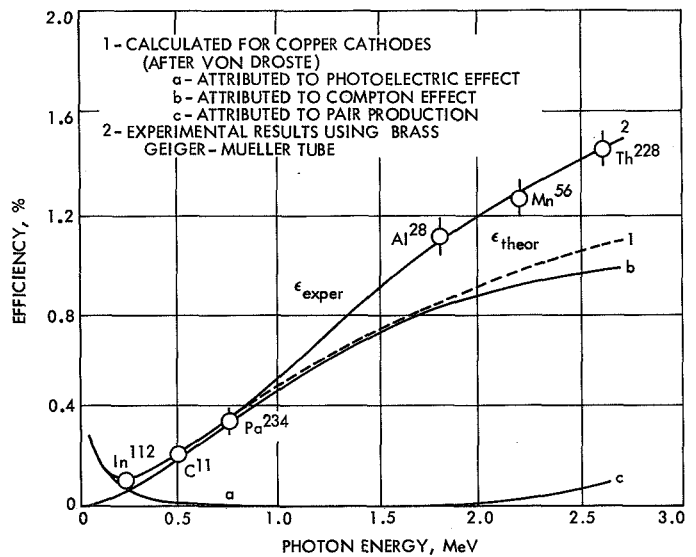


Fig. 5. Experimental curves for the counting efficiency of Geiger-Mueller tubes with brass walls

will attenuate the low-energy photons very strongly and preferentially compared to those more energetic than 0.3 MeV, and because the low-energy gamma photons that reach the counter will have a small effect (see Fig. 4) compared to high-energy gamma photons (> 0.3 MeV).

To calculate the interference in a Geiger counter caused by a gamma flux of known energy spectrum, the flux at each energy is multiplied by the coefficient for secondary electron production in the wall materials. As shown by Fig. 4, stainless-steel walls will have the same coefficient as brass walls for energetic photons above 0.3 MeV. The experimental values for brass walls are available in Fig. 5; these cover most of the range of interest for an RTG. Although the secondary-electron emission coefficient rises rapidly above 3 MeV, it will be seen that the gamma spectrum of an RTG has few photons in the 3- to 7-MeV range; therefore, errors in the extrapolation of the values in Fig. 5 will not impair the usefulness of the method.

C. Photomultiplier Tubes and Channeltrons

Channeltrons are essentially distributed-dynode multipliers acting on the secondary electrons emitted by a target that is associated with (but, that is not an integral part of) the Channeltron. Photomultipliers are a combination of a (generally) low work-function cathode with discrete dynodes that accomplish the electron amplification. Both of these instruments depend on secondary electron emission for their normal operation. They are subject to increased background interference when the gamma-photon flux produced by the RTG causes additional secondary electrons to enter the dynode area. Stainless steel is generally the material of the target, cathode, or other structure that interacts with the gamma-photon flux produced by the RTG—or it may be stainless steel with such a thin coat of platinum or of alkali halides (e.g., lithium fluoride) that the considerations developed for stainless-steel cathodes in Geiger-Mueller tubes hold here also (in respect to response as a function of gamma-photon energy). In the absence of specific experimental data, the coefficients given in Figs. 4 and 5 are useful in estimating the interaction of RTG gamma-photon fields with these detectors.

VI. Neutron and Gamma-Photon Spectra of the RTG

A. Change of Spectrum as a Function of Time

A conceptual design of an RTG, a Martin Marietta Cronus model, is shown in Fig. 6. The present report is based on analyses and conclusions concerning

the postulated application of this RTG unit. Table 9* presents the surface gamma-photon flux in terms of number of gammas/cm²-s in any of 19 energy intervals covering the range of 0.044 to 7 MeV. Similarly, Table 10 presents the surface neutron flux in terms of number of neutrons/cm²-s in any of 23 energy intervals covering the range of 0.025 eV to 10 MeV. The analysis leading to the data in Tables 9 and 10 is based on available information on the outputs of “nominal” Pu²³⁸, as used in the form of the natural oxide, at an age of 1000 days after separation (thermal loading 4100 W). Some characteristics of “nominal” Pu²³⁸ are given in Table 11.

It should be noted that the radiation calculations of the “nominal” Pu²³⁸ will change with time. A comparison is given in Table 12, where the gamma spectra are redistributed into six groups. Similarly, as the fuel ages and the Pu²³⁸ gamma-photon spectrum changes, the relative backgrounds of different types of detectors will also change with time. The Geiger counters and electron multipliers have a rising background-production vs gamma-photon-energy characteristic, whereas solid-state detectors have a falling background-production vs gamma-photon-energy characteristic.

*Data taken from: Gingo, P. J., *Radiation Analysis of an RTG for the Grand Tour Program*, Jet Propulsion Laboratory, Pasadena, Calif. (internal document).

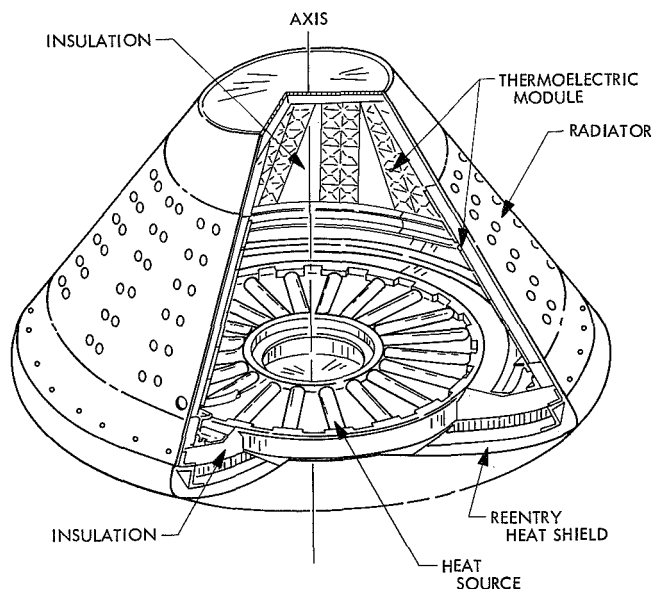


Fig. 6. Conceptual design of an RTG (Martin-Marietta Cronus model)

Table 9. Surface gamma-photon flux of Cronus RTG

Gamma group	Photon energy interval, MeV		Flux at surface, $\gamma/\text{cm}^2\text{-s}$
	From	To	
1	7.0	6.0	3.547×10^0
2	6.0	5.0	1.42706×10^1
3	5.0	4.0	4.31125×10^1
4	4.0	3.0	1.43158×10^2
5	3.0	2.0	5.04436×10^1
6	2.0	1.8	7.27844×10^2
7	1.8	1.6	7.7033×10^2
8	1.6	1.4	3.64511×10^3
9	1.4	1.2	8.18515×10^2
10	1.2	1.0	8.81518×10^2
11	1.0	0.9	3.14254×10^3
12	0.9	0.8	6.6039×10^4
13	0.8	0.7	1.067313×10^5
14	0.7	0.6	3.46538×10^4
15	0.6	0.5	3.7961×10^4
16	0.5	0.4	3.71531×10^4
17	0.4	0.3	3.72378×10^4
18	0.3	0.2	3.24770×10^4
19	0.2	0.044	3.09279×10^4

Table 10. Surface neutron flux of Cronus RTG

Neutron energy interval, MeV		Flux at surface, ^a $n/\text{cm}^2\text{-s}$
From	To	
10.0	8.55	2.676×10^2
8.55	6.66	6.334×10^2
6.66	5.18	1.1658×10^3
5.18	4.46	1.1969×10^3
4.46	4.04	1.8634×10^3
4.04	3.14	9.154×10^3
3.14	2.45	1.2426×10^4
2.45	1.91	8.24166×10^3
1.91	1.49	6.63255×10^3
1.49	1.16	4.3295×10^3
1.16	0.90	2.96783×10^3
0.90	0.702	1.95293×10^3
0.702	0.546	1.19117×10^3
0.546	0.331	1.05256×10^3
0.331	0.201	3.74656×10^2
0.201	0.122	1.4489×10^2
0.122	0.0449	9.2110×10^1
0.0449	0.017	1.88287×10^1
0.017	5.55×10^{-4}	6.7376×10^0
5.55×10^{-4}	3.0×10^{-5}	6.03333×10^{-2}
3.0×10^{-5}	3.0×10^{-6}	1.85847×10^{-5}
3.0×10^{-6}	1.0×10^{-7}	2.3988×10^{-7}
1.0×10^{-7}	2.5×10^{-8}	2.51633×10^{-8}

^aIntegrated flux = $5.37123 \times 10^4 n/\text{cm}^2\text{-s}$
 = $34.65 \times 10^4 n/\text{in.}^2\text{-s}$.

The gamma-photon and neutron field values given in Tables 9 and 10 represent the flux at the surface of the RTG. The fields at points removed from the surface decrease rapidly with separation distance. Figure 7 illustrates the fractional radiation intensity at varying distances from the Cronus RTG surface-reference plane. It will be noted that the decrease is greater for the neutron field, as the separation is increased, than for the gamma-photon field for the same separation. This can be attributed to the fact that neutrons are scattered much less than gamma photons in the body of the Cronus RTG. The neutron field is essentially generated from a concentrated area at the plane of the heat source. The gamma-photon field is generated from a distributed source in the volume between the plane of the heat source and the plane of the surface (outside face) of the Cronus RTG (see Fig. 6).

The relative distribution of gamma photons with energy changes markedly with time after separation of the plutonium fuel; this is primarily because of the small residue

Table 11. Characteristics of RTG-grade Pu²³⁸

Specific neutron yields from light element impurities in "nominal" Pu ²³⁸	
Element	n/s for 1 part/10 ⁶
Li	4.6
Be	133
B	41
C	0.2
N	0.0 ^a
O (natural)	0.1
O ¹⁸	50
F	18
Na	2.2
Mg	2.1
Al	1.0
Si	0.2
P	0.03
S	0.03
Composition of "nominal" Pu ²³⁸	
Isotope	Quantity, %
Pu ²³⁸	81
Pu ²³⁹	15
Pu ²⁴⁰	2.9
Pu ²⁴¹	0.8
Pu ²⁴²	0.1
Pu ²³⁶	0.0001

^aThreshold too high.

Table 12. Gamma-photon spectra for RTG at various times after plutonium separation (normalized to 1.0 for the 0.5- to 1.0-MeV energy interval at 18 yr)

Photon energy interval, MeV		Photons/cm ² -s				
		0 yr	1 yr	5 yr	10 yr	18 yr
From	To					
0.04	0.5	0.12	0.16	0.56	0.90	1.0
0.5	1.0	0.23	0.25	0.30	0.33	0.35
1.0	2	0.096	0.096	0.096	0.096	0.096
2	3	0.003	0.018	0.18	0.32	0.37
3	5	0.0003	0.0003	0.0003	0.0003	0.0003
5	7	0.00003	0.00003	0.00003	0.00003	0.00003

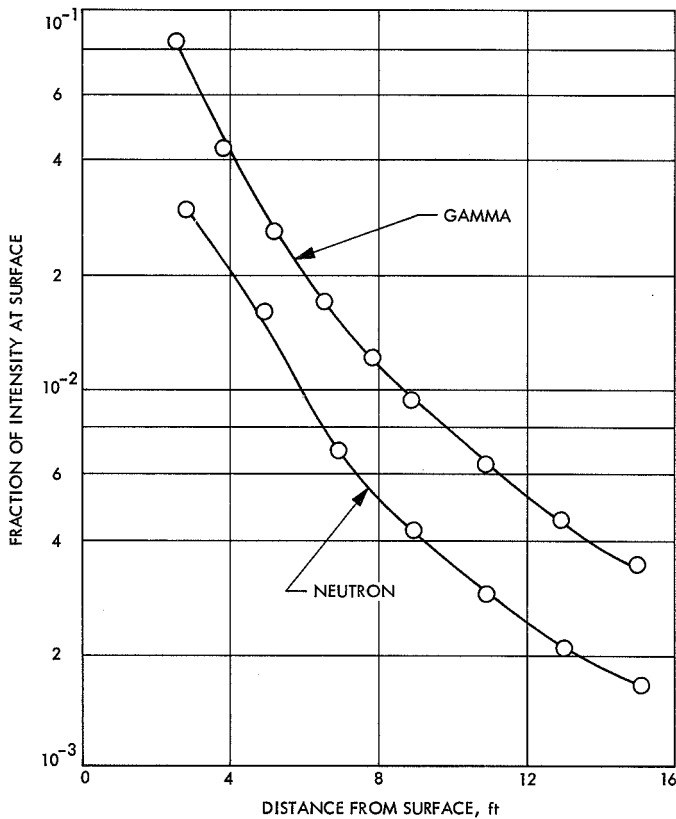


Fig. 7. Gamma and neutron field intensity at various distances from the RTG

of Pu²³⁸ found in the fuel (see Table 11). The spectra, at different times after separation of the fuel ($t = 0, 1, 5, 10, 18$ yr), are shown in Fig. 8 and Table 12. The major changes take place in the 0.2- to 0.3- and the 2- to 3-MeV intervals. The first interval is not of great importance because it is easily shielded. The second, primarily the 2.62-MeV ThC'' gammas, is difficult to shield because (as can be seen in Fig. 9) the minimum mass absorption coefficient μ/ρ (where ρ is the density of the material)

for high-Z shielding material is at 3 MeV. The circuit components (including Geiger-Mueller tube, Channeltron, and photomultipliers) will be subject to increasing background interference as the fuel ages, whereas those components involving solid-state detectors will be less affected because of the low sensitivity of these circuit elements to high-energy radiation.

B. Modification of Spectrum by Shielding

While the elements of the science experiments will be located within the radiation field of the RTG, the intensity at the experiment will be lower than the intensity at the surface of the RTG because of the physical

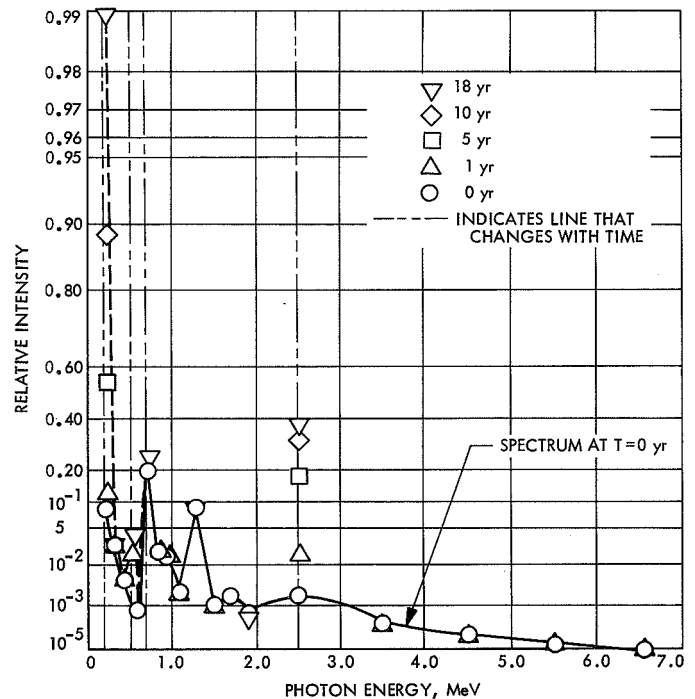


Fig. 8. Gamma-photon spectrum at various times after separation of the Pu²³⁸ fuel

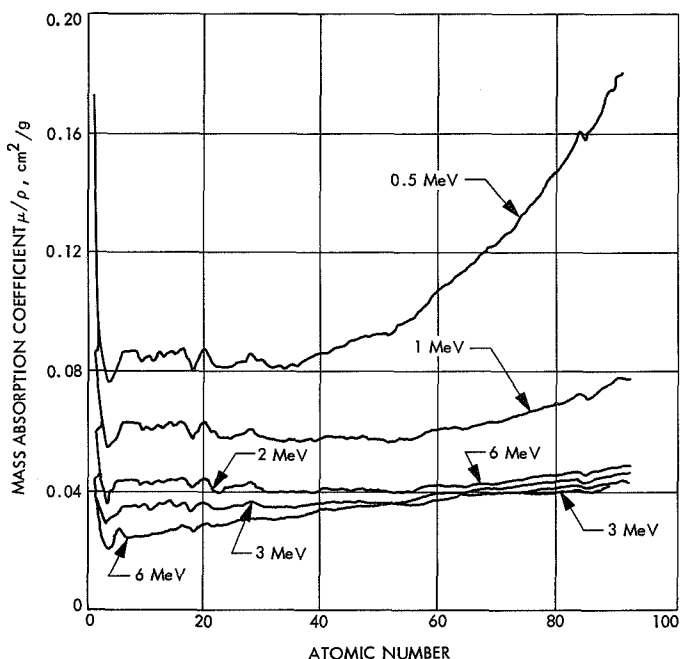


Fig. 9. Mass absorption coefficients between 0.5 and 6 MeV as a function of atomic number

separation and the use of heavy-metal shielding (see Fig. 7). Interposing metal as shielding between instruments and RTG also decreases the radiation fields; for this purpose, tungsten ($Z = 74$, density = 19 g/cm^3) or uranium (natural uranium, depleted of U^{235} and U^{238} , $Z = 92$, density = 18.5 g/cm^3) are the most satisfactory. The computations in this report are based on the use of tungsten shielding, although (as can be seen from Table 13) additional effectiveness can be obtained by the use of uranium shielding because the mass-absorption coefficient is about 50% higher for the same mass per square centimeter in the range of 0.2 to 0.6 MeV. The relative advantage decreases as the energy approaches 3 MeV, but it is still appreciable.

As the neutron flux penetrates the metal shielding, it is somewhat attenuated; in the process of capturing and

Table 13. Mass-absorption coefficients for uranium μ'_U and tungsten μ'_W for the 0.2- to 8-MeV energy interval

Photon energy, MeV	μ'_W	μ'_U	μ'_U/μ'_W
0.2	0.747	1.20	1.61
0.3	0.310	0.470	1.53
0.4	0.184	0.273	1.48
0.5	0.131	0.185	1.41
0.6	0.105	0.142	1.35
0.8	0.079	0.099	1.25
1.0	0.0655	0.078	1.19
1.5	0.0501	0.056	1.12
2.0	0.0432	0.0483	1.12
3.0	0.0400	0.0435	1.09
4.0	0.0400	0.0438	1.09
5.0	0.0409	0.0455	1.11
6.0	0.0426	0.0471	1.11
8.0	0.0449	0.0501	1.12

removing neutrons from the flux, however, additional gamma photons (called "capture gammas"), with a characteristic spectral distribution, are created. In practice (tungsten shielding ≤ 1 in.), the total number of capture gammas is somewhat under 1% of the number of total emerging gamma photons (Table 14). If depleted uranium were used as shielding, the number of capture gammas would be roughly doubled, ranging up to 2% of the total emerging gamma photons, although of somewhat lower maximum energy.

The absolute number of capture-gamma quanta increases with additional shielding up to $\frac{3}{4}$ in. of shielding or 31 g/cm^2 , as shown in Fig. 10. Figure 11 shows the spectral distribution of the total gamma field—including direct gamma photons and capture gamma photons from tungsten shielding for shields of 0, 11, 21, 31, and 42 g/cm^2 (0, $\frac{1}{4}$, $\frac{1}{2}$, $\frac{3}{4}$, and 1 in.)—for a Cronus RTG using 1000-day-old fuel.

Table 14. Contribution of capture gammas produced in tungsten shielding to total emerging gamma photons

Shielding		Contribution as a function of distance (ft) from surface, %						
in.	g/cm^2	0	3	6	9	12	15	Overall 3-15
$\frac{1}{4}$	10.7	0.08	0.035	0.038	0.0365	0.036	0.039	0.036
$\frac{1}{2}$	21.5	0.22	0.095	0.105	0.10	0.10	0.11	0.10
$\frac{3}{4}$	31.2	0.46	0.2	0.22	0.21	0.21	0.225	0.21
1	43	0.90	0.39	0.43	0.41	0.41	0.44	0.41

VII. Shielding Requirements and Effectiveness

A. Optimization of Shielding Weight

The individual science experiments differ in their relative response to low- vs high-energy gamma photons. Therefore, they are individually evaluated to determine the optimum combination of physical separation and shielding to give the best background-interference reduction. The science experiments involving Channeltron, photomultiplier, and Geiger-counter components exhibit a relative response-vs-gamma-photon energy, as shown in Fig. 12. This was obtained by a point-by-point multiplication of the factors taken from Fig. 5 by the total gamma-photon spectrum of Fig. 11. It will be noted that the relative contribution of the 0.7 MeV component is three times that of the 2.62 MeV component when unshielded. This drops to equal contributions (but low absolute values) when 1 in. of shielding is used. A similar point-by-point multiplication for the response in solid-state detectors, using the data of Table 8 and Fig. 11, results in the relative response for silicon given in Fig. 13. In the same manner, Fig. 14 shows the relative response of germanium solid-state devices vs gamma-photon energy in relation to tungsten-shield thickness.

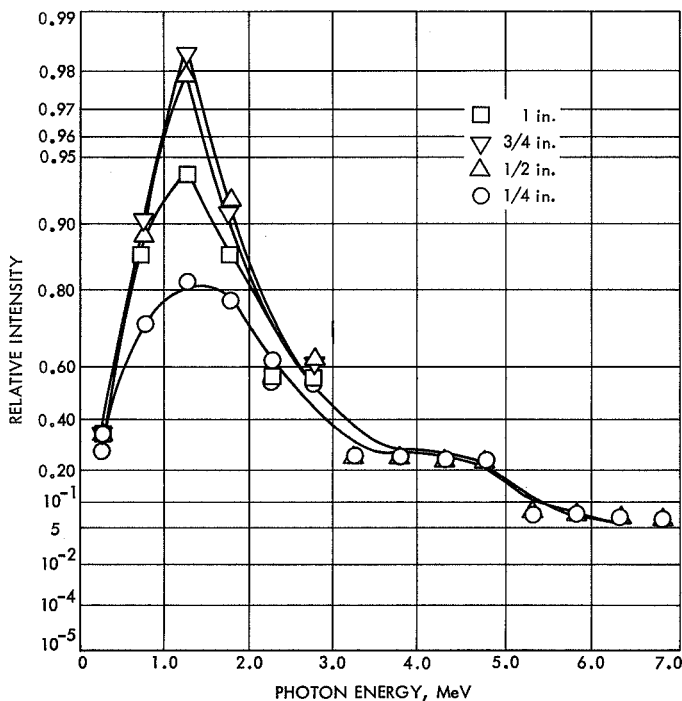


Fig. 10. Intensity distribution of gamma photons produced by neutron-flux interaction with various thicknesses of tungsten

Because the relative response to the low- and the high-energy gamma-photon radiation for the Channeltron and the Geiger counter is different from that for the solid-state detectors, the relative amounts of shielding needed for the two types of detectors will change as the fuel ages, and the shielding required must be calculated separately.

B. Shielding Requirements

Some useful approximations concerning the relationship between the dose rate, the flux intensity, and the source emission rate of gamma photons are listed below:

- (1) From a point source at a distance of 1 ft,

$$D = 6 C E$$

$$D = 1.5 N E \times 10^{-10}$$

$$D = W \times 10^8$$

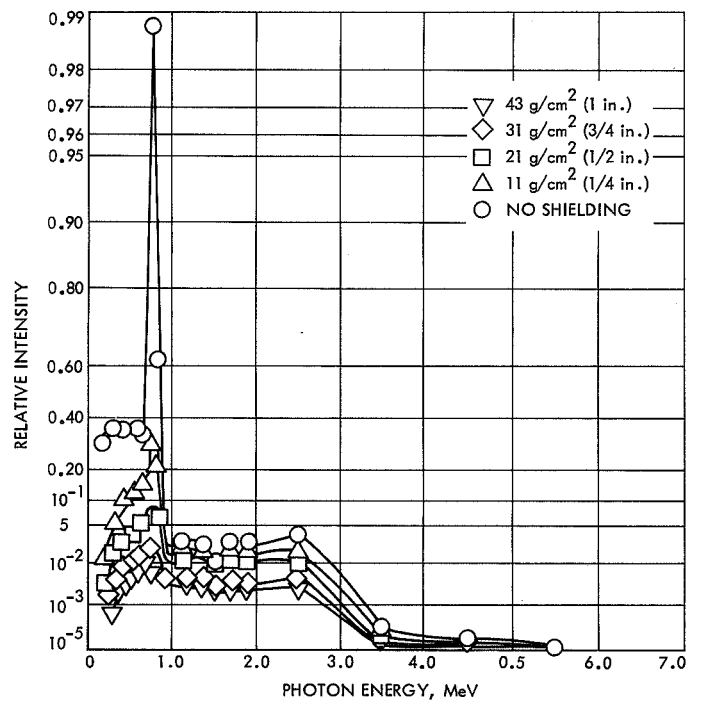


Fig. 11. Total gamma-photon field of RTG for various thicknesses of tungsten (sum of total emerging and capture gammas)

(2) From a gamma-photon flux passing through an absorber,

$$D = 2\phi E \times 10^{-6}$$

$$D = 1.1Q \times 10^7$$

$$D = 1.2Q' \times 10^4$$

where

D = dose rate in R/h

C = curie (defined as the emission of 3.7×10^{10} photons/s)

E = photon energy in MeV

N = total number of gamma photons/s emitted from a point source into 4π steradians

ϕ = gamma-photon flux in photons/cm²-s

W = watts of gamma-photon energy emitted from a point source into 4π steradians

Q = watts of gamma-photon energy/cm²

Q' = watts of gamma-photon energy/ft²

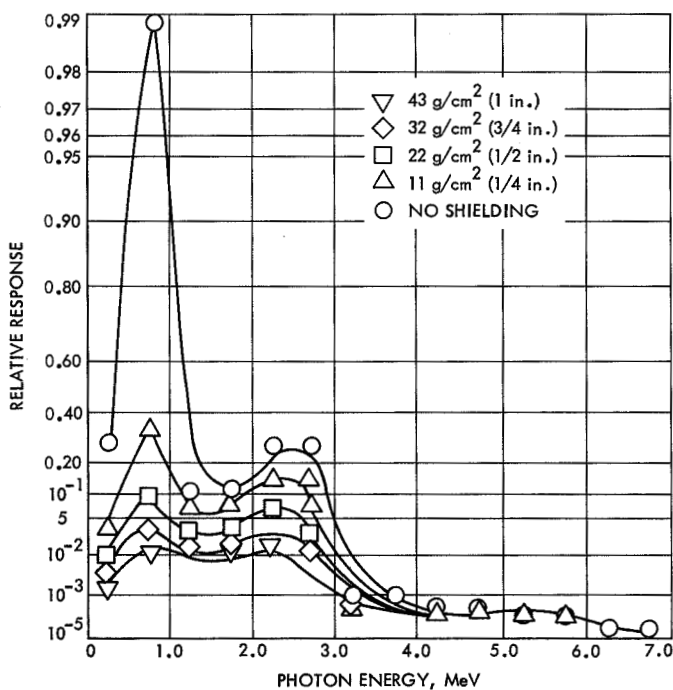


Fig. 12. Relative response vs gamma-photon energy for Geiger counters and Channeltrons with various thicknesses of tungsten

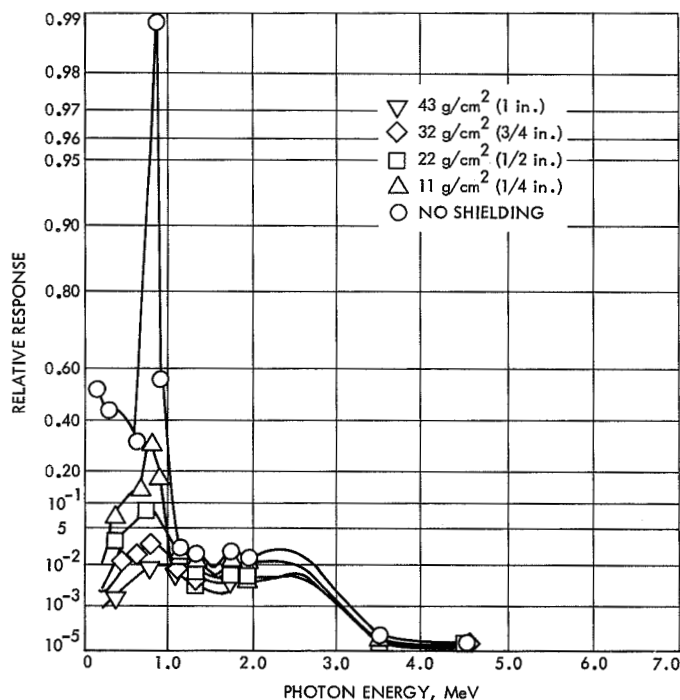


Fig. 13. Relative response vs gamma-photon energy for silicon solid-state detectors with various thicknesses of tungsten

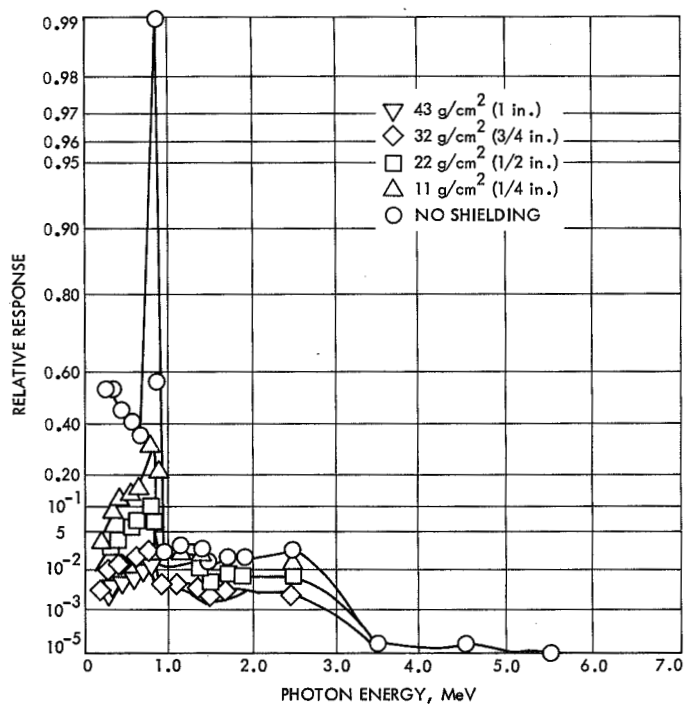


Fig. 14. Relative response vs gamma-photon energy for germanium solid-state detectors with various thicknesses of tungsten

The approximations given above are valid for gamma-photon streams from 0.08 to about 10 MeV, which covers the range of interest in RTG work. For ranges outside these limits, Figs. 15 and 16 give the relationships between dose rate and flux rate, respectively, from 0.01 to 10 MeV.

1. Channeltrons and Geiger counters. These detecting elements, which are used in the LEPEDA and in the UV photometer (see Table 5), respond to the background gamma-photon field of the RTG by registering counts that originate from secondary electrons being ejected from the sensitive area of their inner surfaces.

As discussed in Section V-B, the flux of gamma photons at each energy level can be multiplied by the coefficient for secondary electron production in the wall material to get the number of secondary electrons created per square centimeter of detector surface. If this number is then multiplied by the sensitive area of the detector and by the efficiency η for Channeltron and Geiger counters, the number of background counts contributed by the RTG is obtained.

The surface gamma-photon flux of a Cronus RTG has been calculated for 1000-day-old fuel (see Table 9) in each of 19 energy groups. The effect of shielding on this 1000-day-old fuel/gamma-photon spectrum has also been

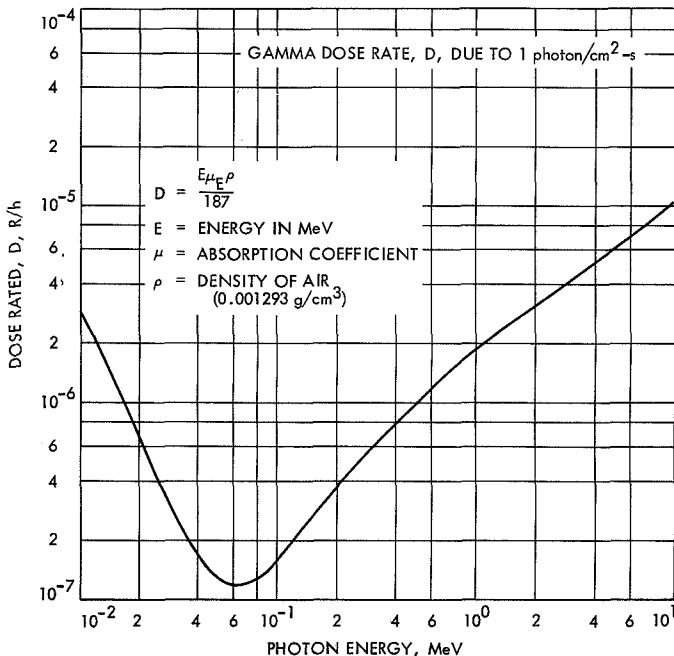


Fig. 15. Dose rate vs photon energy (0.01-10 MeV)

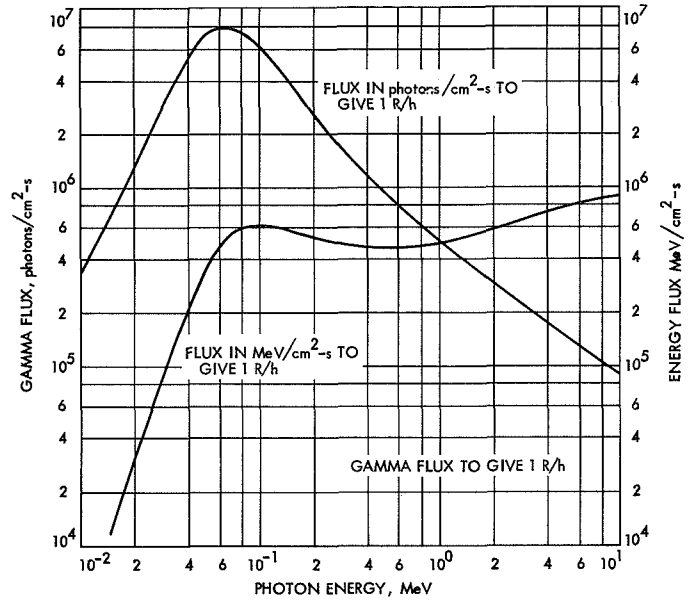


Fig. 16. Photon flux vs energy (0.01-10 MeV)

calculated; Table 15 shows the ratio of emerging to incident gamma-photon flux, for each of the energy intervals, for tungsten shielding of 1/4-, 1/2-, 3/4-, and 1-in. thicknesses.

The following expression gives the background interference contributed by the Cronus RTG to the Channeltrons and the Geiger counters:

$$R = \sum \eta \phi(E) \tau(E, x) \beta(E) f(d) A$$

where

R = background counting rate in counts/s

η = efficiency of counting of ejected secondary electrons (may be taken to be 100%)

ϕ = gamma-photon flux at RTG surface in photons/cm²-s as a function of energy (see Table 9)

τ = transmission of tungsten shield of thickness x as a function of energy (see Table 15)

β = secondary-electron emission coefficient as a function of energy (see Figs. 5 and 17)

f = fraction of surface-gamma intensity at a distance d from the RTG surface (see Fig. 7)

A = sensitive area of detector projected normal to flux

Table 15. Ratio of emerging to incident gamma-photon flux

Gamma-photon energy group	Photon energy interval, MeV		Tungsten shielding thickness, in.			
	From	To	1/4	1/2	3/4	1
1	7.0	6.0	0.488396	0.246872	0.124788	0.063077
2	6.0	5.0	0.501611	0.259959	0.134713	0.069812
3	5.0	4.0	0.529117	0.275563	0.143513	0.074741
4	4.0	3.0	0.5332425	0.291904	0.1599416	0.087472
5	3.0	2.0	0.5509065	0.310222	0.174690	0.098370
6	2.0	1.8	0.578643	0.335551	0.194584	0.11284
7	1.8	1.6	0.59008	0.345754	0.202592	0.118708
8	1.6	1.4	0.776588	0.528617	0.359826	0.24493
9	1.4	1.2	0.600504	0.3541249	0.208832	0.1231509
10	1.2	1.0	0.619755	0.350511	0.1982363	0.112115
11	1.0	0.9	0.694115	0.438556	0.2770886	0.17507
12	0.9	0.8	0.339859	0.120187	0.042503	0.01503
13	0.8	0.7	0.313607	0.101831	0.033065	0.010737
14	0.7	0.6	0.42779	0.172389	0.069469	0.0279942
15	0.6	0.5	0.349534	0.13209	0.04992	0.018864
16	0.5	0.4	0.274280	0.0991556	0.03585	0.012959
17	0.4	0.3	0.156970	0.055515	0.019633	0.006943
18	0.3	0.2	0.055205	0.020106	0.007323	0.002667
19	0.2	0.044	—	—	—	—

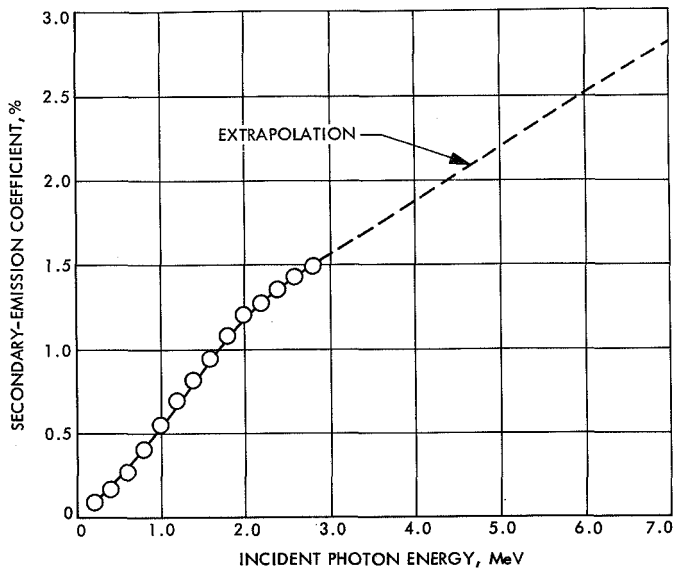


Fig. 17. Secondary electron emission coefficient (extrapolated from Fig. 5 data)

The product of the first four terms ($\eta \phi \tau \beta$) has been evaluated for each energy group of Table 9 and for each thickness shown in Table 15, and the totals for each thickness determined. The mass-absorption coefficient (see Fig. 9) for heavy metals such as tungsten ($Z = 74$)

preferentially attenuates gamma radiation under 2 MeV and over 5 MeV, and is least effective for the important gamma-photon energy group 5 (2 to 3 MeV) of Table 9. The ratios of the quantity $\eta \phi \tau \beta$, evaluated for successive 1/4-in. shield slab thicknesses, converge quickly to the theoretical value for the 2.62-MeV gamma photon of ThC'', which is the unique spectral line from the decay product of the Pu²³⁸ impurity that gives rise to gamma-photon energy group 5. The convergence is so rapid (Fig. 18) that extrapolated values may safely be used to predict the effect of tungsten shielding thicker than 1 in. With the use of extrapolated values, the effect of tungsten shielding in the range of 0-2 1/2 (0-108 g/cm²) on the spurious counting rate (with no separation in distance from the RTG) for Channeltrons and Geiger counters is given in Table 16. (The volume of 1 cm³ of tungsten has a mass of 17 g, and a slab 1 cm² × 1/4 in. has a volume of 10 × 10 × 6.35 mm = 0.635 cm³ or 10.8 g.)

To arrive at the amount of shielding required for Channeltron detectors, it should be noted that the sensitive area of the Channeltron is the initial section of the tube. According to the manufacturer of the Channeltron 4010 tube, omission of the gain of the first 15% of the length of the tube decreases the output of the tube to 10% of its design value. Therefore, it will be sufficient to shield only this initial 15% of the 4-in. length, or

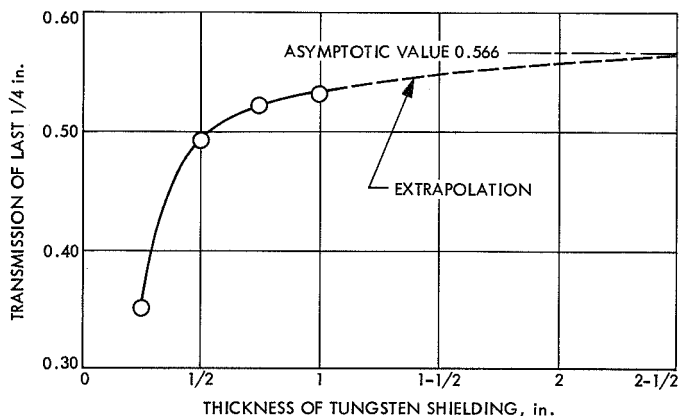


Fig. 18. Effect of 1/4-in. increments of tungsten shielding on the ratio of spurious counts in Geiger counters and Channeltrons

0.6 in. The inside diameter of the Channeltron 4010 is 0.040 in. To determine the effective sensitive area, it will be noted that the penetration of secondary electrons of 3-MeV energy is 2 g/cm², and that this represents a wall thickness of 0.1 in. for material of the density of steel or brass (correspondingly more for lower-density wall material). Because secondary electrons of 3-MeV energy represent the upper limit of the secondary-electron energy spectrum that will be produced, the effective sensitive area of the Channeltron can conservatively be assumed to be a strip, 0.6 × 0.040 in., surrounded by a band 0.1 in. on all sides, or a total area of 0.8 × 0.24 in., which is 0.2 in.² or 1.2 cm².

When a Channeltron is used in a science experiment, it is required to measure events when the background counting rate is 5 counts/min or 0.1 count/s. The expression $R = \Sigma \eta \phi \tau \beta f A$ has been evaluated for Channeltrons, and is presented in Fig. 19. From this figure, one can determine the amount of tungsten shielding required to reduce the background interference caused by gamma-photon radiation from the RTG to the required level. If it is necessary to reduce the background counting rate caused by the RTG to a level no greater than the background counting rate for all other causes, it must be reduced to 0.1 count/s for the Channeltron 4010 tube. This requires a separation of 10 ft if 2 in. of tungsten shielding is used. Other separations will require different thicknesses of tungsten, as shown in Fig. 19.

The Geiger-Mueller tubes that are to be used in the science package are thin end-window, miniature, self-quenching tubes (EON-6213). Although the secondary-electron emission coefficient for these tubes (with

Table 16. Effect of tungsten shielding on spurious counting rate for Channeltrons and Geiger counters

Thickness of shielding, in.	Mass of shielding, g/cm ²	Spurious counts after penetrating given shielding thickness, counts/cm ² -s
0	0	2624
1/4	10.8	928
1/2	21.6	459
3/4	32.4	240
1	43.2	128
1 1/4	54.0	69
1 1/2	64.8	38
1 3/4	75.6	21
2	86.4	12
2 1/4	97.2	7
2 1/2	108.0	4

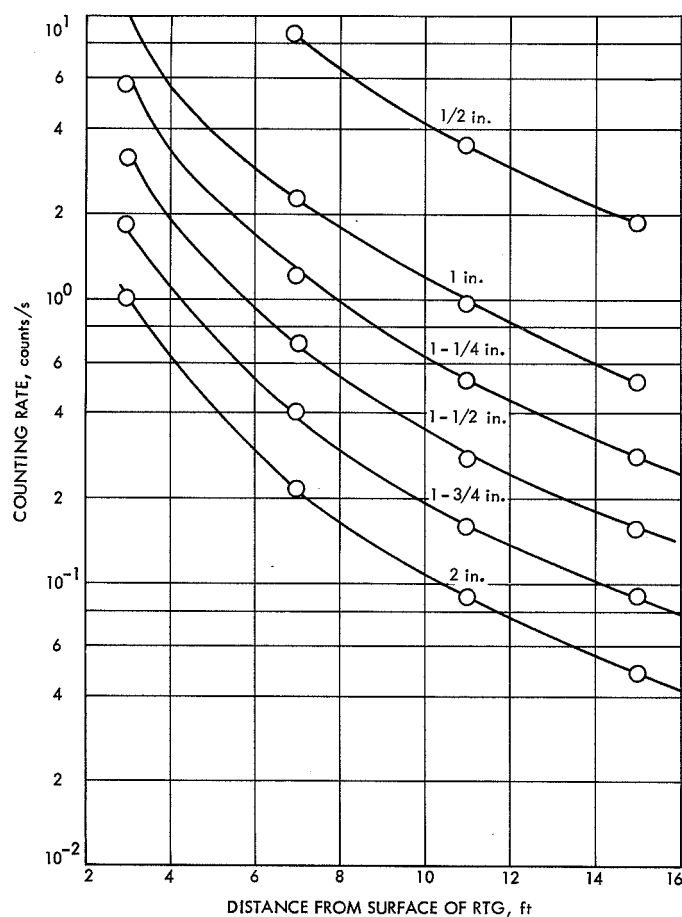


Fig. 19. Background counting rate for Channeltrons (CEM-401, CEM-4010) caused by the Cronus RTG with various thicknesses of tungsten shielding

chromium-iron walls) may be taken to be that given in Fig. 17, the difference in physical size of the sensitive area requires that a separate evaluation be made of separation-distance, shield-thickness, and counting-rate interrelationships. The tube has an inside diameter of 0.093 in. and an effective length of 0.300 in. The determination of the effective sensitive area is found to be physically similar to that for the Channeltron. A conservative assumption is that the effective sensitive area is a strip, 0.093×0.300 in., surrounded by a band, 0.1 in. on all sides, or a total area of 0.293×0.500 in., which is 0.15 in.^2 or 0.96 cm^2 . As was done for the Channeltron, the expression $R = \Sigma \eta \phi \tau \beta f A$ has been evaluated for these tubes; the results are presented in Fig. 20. As an example of the use of this figure, the trapped radiation detector may be considered. In this instrument, the Geiger counters have a specified dynamic counting range of 36 counts/min to 6×10^8 counts/min. If the background interference caused by the RTG is restricted to $\frac{1}{2}$ the minimum dynamic range (i.e., 18 counts/min or 0.3 counts/s), it is seen that $1\frac{1}{4}$ in. of shielding at 13 ft or $1\frac{1}{2}$ in. of shielding at 10 ft is required.

2. Solid-state detectors. Solid-state detectors will be used in the trapped radiation detector and in the cosmic ray telescope (see Table 5). Following the analysis developed in Section V-A, the number of gamma photons absorbed from an impinging beam by a slab of silicon or germanium can be found. This is done by multiplying the gamma-photon flux for each energy interval by the absorption coefficient of the silicon (or germanium) for that energy interval. The gamma-photon flux for each energy interval has been calculated for the Cronus RTG design, for 1000-day-old fuel, and is given in Table 9. The effect of shielding on the gamma-photon spectrum for 1000-day-old fuel has also been calculated; Table 15 shows the ratio of emerging to incident gamma-photon flux, for each of the 20 energy intervals, for tungsten shielding of $\frac{1}{4}$ -, $\frac{1}{2}$ -, $\frac{3}{4}$ -, and 1-in. thicknesses. The absorption coefficients involved have been calculated from the data given in Fig. 3, and are tabulated in Table 8.

To calculate the background interference contributed by the RTG to the solid-state detectors, use is made of the experimental data contained in Ref. 4 and reviewed in Section V-A. It is shown that, for a silicon detector of $100 \text{ mm}^2 \times 500 \mu\text{m}$ (50 mm^3), the number of counts produced was 3.4% of the number of gamma photons absorbed in a 1-cm-thick slab of silicon. The 3.4% value held at both 0.1 and 0.4 MeV, and may be assumed to be valid for the entire spectrum of interest.

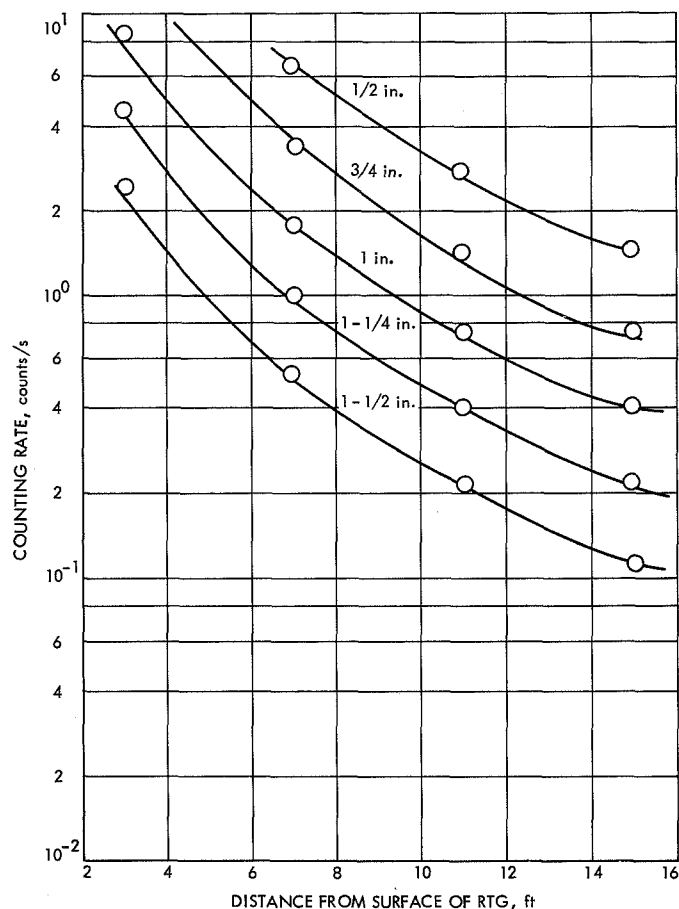


Fig. 20. Background counting rate for Geiger-Mueller tube (EON-6213) caused by the Cronus RTG with various thicknesses of tungsten shielding

The product $\Sigma \phi_E \mu_E$, where ϕ_E is the flux rate for gamma photons of energy E and μ_E is the absorption coefficient for gamma photons of energy E , was evaluated for the energy ranges given in Table 9 for a bare Cronus RTG, and for the shielding-modified flux given in Table 15. The values of μ_E were taken from Table 8. The number of counts to be expected from a $1\text{-cm}^2 \times 500\text{-}\mu\text{m}$ detector was then calculated for each shield thickness, and is presented in Table 17.

The effect of shielding on flux-energy distribution was only carried out to 1 in. of tungsten in Table 15; however, an extrapolation of the effectiveness of each additional $\frac{1}{4}$ -in. increment of tungsten shielding was made, as shown in Fig. 21, and allowed the Table 17 data to be carried out to $2\frac{1}{2}$ in. of shielding. A similar extrapolation can be made with germanium solid-state detectors (Table 18) when a one-point experiment can be performed to determine the conversion efficiency of germanium. At

Table 17. Effect of tungsten shielding on spurious counting rate for silicon solid-state detectors

Thickness of shielding, in.	Mass of shielding, g/cm ²	Gamma photons absorbed, ^a photons/cm ² -s	Counts detected, ^b counts/s
0	0	25,815	878
¼	10.8	6,839	233
½	21.6	2,777	94
¾	32.4	1,214	41
1	43.2	562	19
1¼	54.0	278	9.5
1½	64.8	142	4.8
1¾	75.6	74	2.5
2	86.4	40	1.4
2¼	97.2	21	0.7
2½	108.0	11	0.37

^aNumber of gamma photons absorbed from the incident beam, per centimeter travel through silicon detector, per square centimeter per second. Silicon detector at the surface of the Cronus RTG, the gamma-photon beam having penetrated a given shielding thickness. Number of photons is equal to: $\Sigma \phi_E \mu_E$.

^bNumber of counts per second generated by beam passing through silicon detector 1 cm² × 500 μm. This number is equal to 3.4% of gamma photons absorbed.

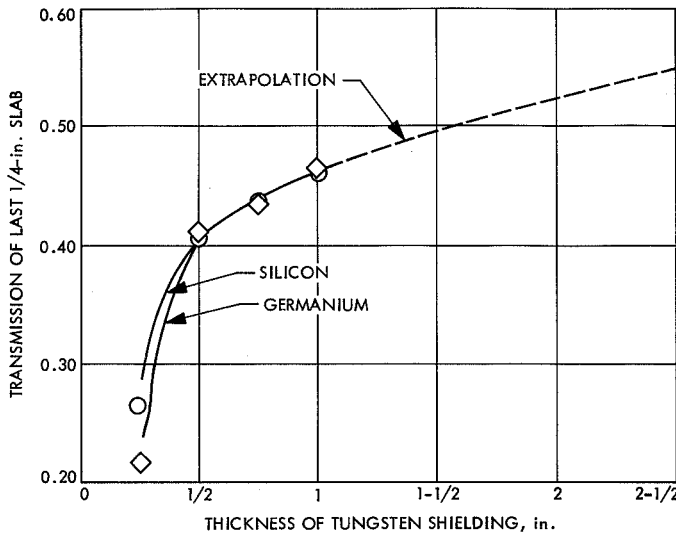


Fig. 21. Effect of ¼-in. increments of tungsten shielding on the ratio of spurious counts in silicon and germanium solid-state detectors

present, only silicon solid-state detectors are planned for use in the spacecraft science experiments, and Table 17 gives sufficient information to determine the shielding thicknesses needed.

The information given on the trapped radiation detector has been summarized by Canvel (Ref. 10). The

silicon solid-state detector that was used has a normal sensitive area of 12 mm² and a depth of 31.7 μm. Although the background or minimum needed rate is not quoted, the device has a "weak inflight source" providing 0.05 count/s or less for calibration. If it is assumed that a background of 2% of the calibration strength is acceptable, shielding and distance must be adjusted to give 0.001 count/s from the RTG. Calculations based on Table 17, taking into account that the present silicon cell has a volume of 12 mm² × 31.7 μm, or only 0.0076 that of the cell discussed in Ref. 4, and including the effect of separation distance (see Fig. 7), leads directly to Fig. 22, which shows background-separation relationships for several shield thicknesses.

The other experiment cited, the cosmic ray telescope, is described in Ref. 11. The referenced publication indicates that the silicon detectors that are to be used will have a surface area of 5.7 cm² and a depletion depth of 200 μm. This value is 2.28 times that used in Ref. 4, and the counting rate to be expected, based on the data tabulated in Table 17, must be multiplied by this factor for each shielding thickness.

A background counting rate of 1 count/s will be under 10% of the minimum value of interest, and is suggested here as a tolerable RTG background. The background-vs-separation relationship is shown, for several thicknesses of shielding, in Fig. 23.

Table 18. Effect of tungsten shielding on the number of gamma photons absorbed from incident beam by a germanium slab

Thickness of shielding, in.	Mass of shielding, g/cm ²	Gamma photons absorbed, ^a photons/cm ² -s
0	0	72,416
¼	10.8	15,701
½	21.6	6,451
¾	32.4	2,808
1	43.2	1,308
1¼	54.0	647
1½	64.8	329
1¾	75.6	172
2	86.4	90
2¼	97.2	48
2½	108.0	26

^aNumber of gamma photons absorbed from the incident beam, per centimeter travel through germanium detector, per square centimeter per second. Germanium detector at the surface of the Cronus RTG, the gamma-photon beam having penetrated a given shielding thickness. Number of photons is equal to: $\Sigma \phi_E \mu_E$.

C. Summary

Table 19 gives a summary of the required sizes and thicknesses of shielding to keep the background rates of the individual experiments within the proposed limits. The practical size of each spot shield depends on the individual experiment and its container, taking into account the accessibility of the components. Under some circumstances, a spot shield might be reduced in size, but such reduction depends on a detailed analysis of the container and enclosure for each experiment. The data in Table 19 are based on Figs. 19, 20, 22, and 23.

As was pointed out earlier in this report, the use of depleted uranium as shielding in place of tungsten can be expected to reduce the weight of the shielding somewhat (compare Fig. 9 and Table 13).

VIII. Current Programs

Work on determining the necessary shielding from RTG radiation for spacecraft components and science experiments is continuing at JPL. To define the problem adequately, it is necessary to examine optimization of individual spacecraft configurations and science-experiment components with a physical position layout. The specific experiment configurations and their sizes, packaging, and disposition have an important bearing on the weight of the shielding required.

Further evaluation of shielding requirements will consider the necessary sensitivity of the science-experiment instruments and the allowable spurious counting rate of the detectors and detector systems involved. From these

Table 19. Weight of shielding required for science experiments in the vicinity of the Cronus RTG

Detector parameters	LEPEDEA ^a		UV photometer		Trapped radiation detector		Cosmic ray telescope
	Channeltron	Geiger counter	Channeltron	Geiger counter	Solid state (12 mm ² × 31 μm)	Geiger counter	Solid state (5.7 cm ² × 200 μm)
Number required per experiment	2	1	1	1	1	3	1
Sensitive area to be protected, cm ²	1.2	1.0	1.2	1.0	0.12	1.0	5.7
Proposed spot shield size, cm ²	6	4	10	4	3	4	10
Background rate acceptable, counts/s	0.1	0.3	0.1	0.3	0.001	0.3	1
Tungsten shielding required	2	1½	2	1½	1	1½	¾
11 ft in. g/cm ²	86.4	64.8	86.4	64.8	43.2	64.8	32.4
15 ft in. g/cm ²	1¾	1¼	1¾	1¼	¾	1¼	½
Individual shield weight at 11-ft separation, g	75.6	54.0	75.6	54.0	32.4	54.0	21.6
Individual shield weight at 15-ft separation, g	518	259	864	259	130	259	324
Total shield weight at 11 ft, g	1036	259	864	259	130	777	324
Total shield weight at 15 ft, g	454	216	756	216	97	216	216
Total shield weight at 11-ft separation	908	216	756	216	97	648	216
Total shield weight at 15-ft separation	3649 g (8.03 lb)						
	3057 g (6.73 lb)						

^aLEPEDEA = low-energy proton and electron differential energy analyzer.

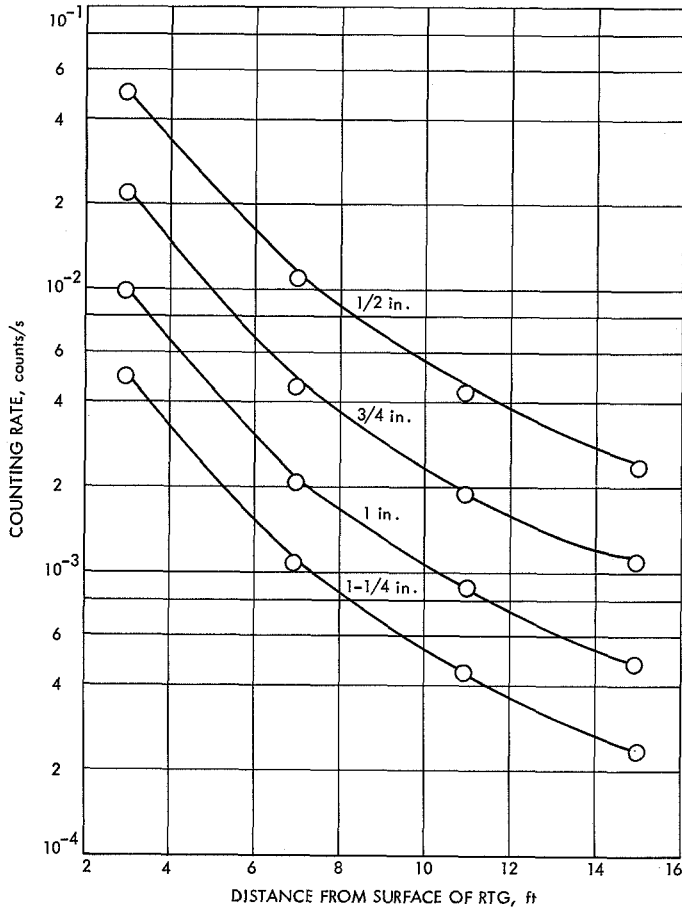


Fig. 22. Background counting rate for 12-mm² × 31.7-μm silicon cell caused by the Cronus RTG

data, configuration of the shielding required can be specified in greater detail, and more subtle effects (such as the interaction from scattered radiation from structural members of the spacecraft on the experiments) can be evaluated.

Concurrent analytical and experimental programs are underway to carry out these evaluations. The empirical evaluations of the sensitivities of the possible sensors, as presented in the preceding pages, are being supplemented by an analytical program using Monte Carlo techniques to determine sensor responses to predicted

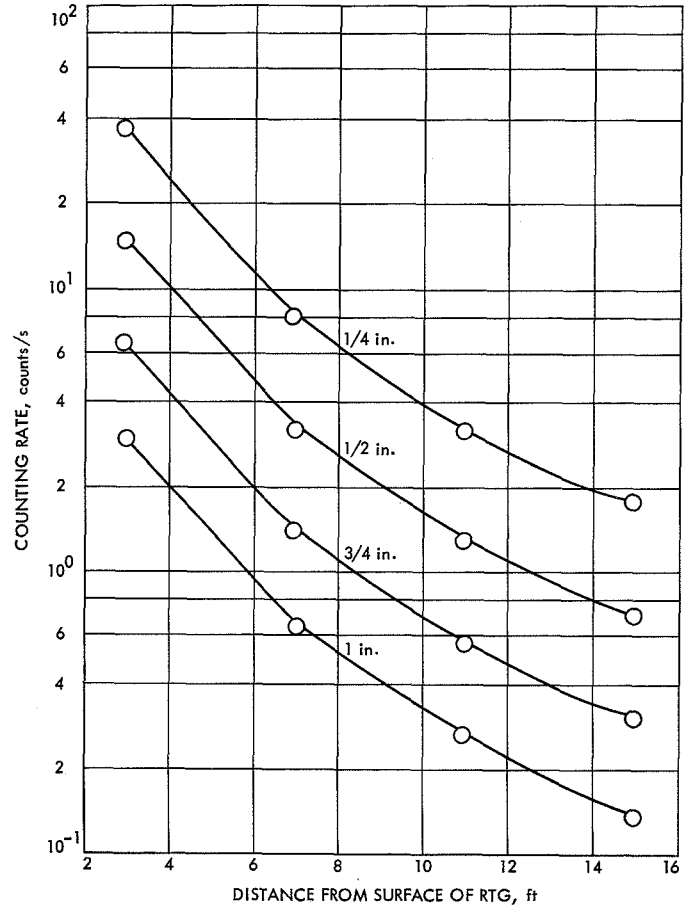


Fig. 23. Background counting rate for 5.7-cm² × 200-μm silicon cell caused by the Cronus RTG

radiation fields. At the same time, further evaluation of the actual response of sensors and detectors is being done through an extended experimental program. One part of the experimental program is to irradiate various sensors and determine the practical sensitivity vs energy of gamma and neutron fields (this is being done by an independent outside contractor). Work is simultaneously proceeding at JPL to irradiate sensors with continuous spectra to determine interference effects, and to corroborate and guide the analytical studies. Developments in RTG fuels, design, and operation are being monitored so that any improvements can be incorporated into the program.

References

1. Leary, J. A., and Mullins, L. J., *Preparation of Ultra-High Purity Plutonium*, USAEC Report LA-3356-MS. U.S. Atomic Energy Commission, Washington, Aug. 1965.
2. *Mariner Mars 1964 Final Project Report*, NASA SP-139, p. 239. National Aeronautics and Space Administration, Washington, 1967.
3. Frank, L. A., *Low-Energy Proton and Electron Experiment for the Orbiting Geophysical Observatories B and E*, Report 65-22. University of Iowa, Ames, Iowa, July 1965.
4. Jones, A. R., *Gamma Ray Dosimetry with p-i-n Junction Converters*, AECL-2252. Atomic Energy of Canada, Ltd., Chalk River, Ontario, Canada, Feb. 1965.
5. Gradstein, G. W., *X-ray Attenuation Coefficients from 10 Kev to 100 Mev*, NBS Circular 583. United States Government Printing Office, Washington, 1957.
6. Goulding, F. S., "A Survey of the Applications and Limitations of Various Types of Detectors in Radiation Energy Measurement," *IEEE Trans.*, Vol. NS-11, No. 3, pp. 177-190, June 1964.
7. Bradt, H., et al., "Empfindlichkeit von Zahlrohren mit Blei, Messing, und Aluminum-Kathode für γ -Strahlung im Energieintervall 0.1 Mev bis 3 Mev," *Helv. Phys. Acta*, Vol. 19, p. 47, 1946.
8. Maier-Liebnitz, H., "Absolute Zahlrohrmessungen an γ -Strahlen," *Z. Naturforsch.*, Vol. 1, p. 243, 1946.
9. Von Droste, G., "Über die Anzahl der Ausschläge eines Zahlrohres bei Bestrahlung mit γ -Strahlen verschiedener Wellenlänge," *Z. Phys.*, Vol. 100, p. 529, 1936; Vol. 107, p. 474, 1936.
10. Cavel, H., *Trapped Radiation Detector*, Technical Report 32-1197. Jet Propulsion Laboratory, Nov. 15, 1967, Pasadena, Calif.
11. *Instruments and Spacecraft*, NASA SP-3028, p. 739. National Aeronautics and Space Administration, Washington, 1966.